NATIONAL AERONAUTICS AND SPACE ADMINISTRATION

Space Programs Summary 37-51, Vol. I

Flight Projects

For the Period March 1 to April 30, 1968

JET PROPULSION LABORATORY

CALIFORNIA INSTITUTE OF TECHNOLOGY

PASADENA, CALIFORNIA

May 31, 1968

NATIONAL AERONAUTICS AND SPACE ADMINISTRATION
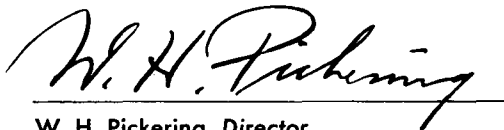
Space Programs Summary 37-51, Vol. I

Flight Projects

For the Period March 1 to April 30, 1968

SPACE PROGRAMS SUMMARY 37-51, VOL. I

Preface

The Space Programs Summary is a bimonthly publication that presents a review of engineering and scientific work performed, or managed, by the Jet Propulsion Laboratory for the National Aeronautics and Space Administration during a two-month period. Beginning with the 37-47 series, the Space Programs Summary is composed of four volumes:

Vol. I.   *Flight Projects* (Unclassified)

Vol. II.   *The Deep Space Network* (Unclassified)

Vol. III.   *Supporting Research and Advanced Development* (Unclassified)

Vol. IV.   *Flight Projects and Supporting Research and Advanced Development* (Confidential)

Approved by:

W. H. Pickering, *Director*
Jet Propulsion Laboratory

PRECEDING PAGE BLANK NOT FILMED.

Contents

PLANETARY—INTERPLANETARY PROGRAM

LUNAR PROGRAM

ADVANCED STUDIES

I. Mariner Mars 1969 Project

PLANETARY–INTERPLANETARY PROGRAM

A. Introduction

The *Mariner* Mars 1969 Project was initiated in late December 1965 and formally tasked on February 1, 1966. The primary objective is to make two flyby exploratory investigations of Mars in 1969, which will set the basis for future experiments—particularly those relevant to the search for extraterrestrial life. The secondary objective is to develop Mars mission technology.

The spacecraft design concept is modeled after the successful *Mariner IV* spacecraft, considerably modified to meet the 1969 mission requirements and to enhance mission reliability.

The launch vehicle is the *Atlas/Centaur* SLV-3C, used for the *Surveyor* missions. This vehicle, developed by General Dynamics/Convair Company for the Lewis Research Center has a single- or double-burn capability in its second stage and a considerably increased performance rating over the *Atlas D/Agena D* used in the *Mariner IV* mission.

Mariner Mars 1969 missions will be supported by the Eastern Test Range launch facilities at Cape Kennedy, the tracking and data acquisition facilities of the Deep Space Network, and other NASA facilities.

The six planetary-science experiments, selected by NASA for the *Mariner* Mars 1969 missions are listed in Table 1.

During March and April 1968 delivery and subsystem testing of proof test model spacecraft equipment were completed. Two system tests of the assembled spacecraft were conducted; other surveys and calibrations were also run. The first space-simulator test was begun late in April.

The initial match-mate test was conducted in San Diego, California in March, using the development test model spacecraft with *Centaur* forward mockup, nose fairing, and handling equipment developed for *Surveyor*. The eighth quarterly project review will be conducted in May.

Table 1. Mariner Mars 1969 scientific investigations

Experiment	Scientific investigator	Affiliation
Television	R. B. Leighton[a]	CIT
	B. C. Murray	CIT
	R. P. Sharp	CIT
	N. H. Horowitz	CIT
	J. D. Allen	JPL
	A. G. Herriman	JPL
	R. K. Sloan	JPL
	L. R. Malling	Massachusetts Institute of Technology
	M. E. Davies	Rand Corporation
	C. Leovy	Rand Corporation
Infrared spectrometer	G. C. Pimentel[a]	UCB
	K. C. Herr	UCB
Ultraviolet airglow spectrometer	C. A. Barth[a]	University of Colorado
	W. G. Fastie	Johns Hopkins University
Infrared radiometer	G. Neugebauer[a]	CIT
	G. Munch	CIT
	S. C. Chase	Santa Barbara Research Center
S-band occultation	A. J. Kliore[a]	JPL
	D. L. Cain	JPL
	G. S. Levy	JPL
Celestial mechanics	J. D. Anderson[a]	JPL

[a]Principal investigator.

B. Project Engineering

1. Launch Vehicle Integration

During this period the initial match-mate test was successfully completed, and the spacecraft/launch vehicle interface design continued to be refined and documented. Technical agreements were made in the following areas:

(1) JPL thermal diaphragm design acceptance.

(2) Air conditioning duct and adapter interface design.

(3) Cross talk control on JPL lines at launch complex 36.

(4) Override control of launch complex 36 main electrical breakers.

(5) Pyrotechnic design verification test-related procedures and $X + 1$ h report of the test.

(6) Match-mate test-related procedures and $X + 1$ h report of the test.

(7) Participation of the Mariner Mars 1969 spacecraft in the combined readiness test.

(8) Nose fairing clearance and alignment problems.

Match-mate testing was conducted at General Dynamics/Convair, San Diego, on March 11–14, 1968; the development test model spacecraft and Mariner adapter were mated with a dummy Centaur forward bulkhead and Surveyor-type nosefairing, with Surveyor ground handling equipment. Launch type encapsulation and mating were accomplished, followed by pressurization checks and X-ray determination of physical clearances. Then, in a simulated nose-fairing jettison, the full-length shroud halves were separated and rotated away from the mated vehicle (Fig. 1). Although scheduled for 10 days, the series was successfully concluded within 4 days.

The pyro design verification test was successfully conducted at General Dynamics/Convair from late March to early April 1968. A number of runs simulating Centaur/Mariner separation and prelaunch testing were conducted, using live squibs, resistive simulators, and a relay-box simulator (to be used in ground tests at Cape
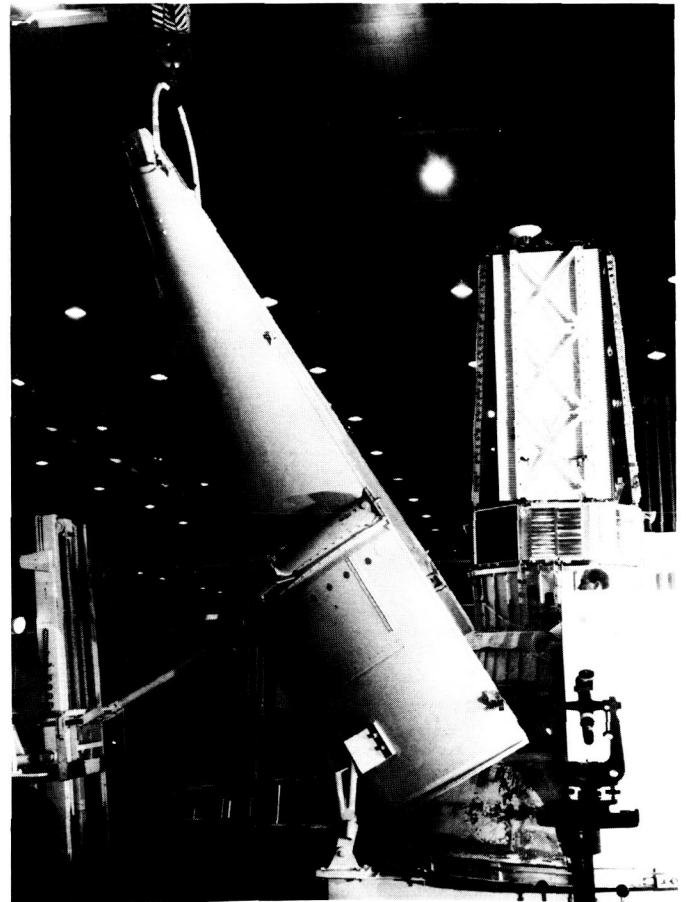

Fig. 1. Nose fairing rotation during match-mate operations

Kennedy) with a launch vehicle type relay-box and power source.

2. System Integration

a. Spacecraft power margins. The latest information regarding solar panel performance and spacecraft power demands during encounter and playback is given in Table 2. The solar panel capability is 464 W, minimum guaranteed power at encounter without degradation as measured at the power source logic input. Demands are those computed from the latest power profile.

The columns labelled "maximum flare" are based on the assumption of 17% degradation from the "no-flare" performance. Calculations for 16 days past encounter are based on a performance capability of 0.9285 of the encounter capability due to reduced solar intensity to which is added a correction factor of 9.9 W (no flare) or 8.2 W (maximum flare) resulting from an estimated temperature drop of 5°C. All margins are then rounded to the nearest watt.

b. Battery test load. A battery test load has been incorporated into the spacecraft system design to permit in-flight assessment of the condition of the battery. The load is a 15-W resistor connected to the battery, or disconnected, in response to a DC-50 command. Telemetry readings of battery current and voltage, with and without the test load, constitute the assessment.

The resistor is to be located in Bay II of the spacecraft bus, which contains the propulsion subsystem; the exact location is being studied. A secondary function of the load is to heat the propellant tank, if necessary, to prevent the propellant from freezing late in the mission.

The power dissipated by the test load was constrained to be somewhat less than the capability of the battery charger (18 W), so that, if a failure occurred such that the test load could not be disconnected, the battery charger would still be capable of supplying enough current to keep the battery charged. The test load had to be sufficiently large to provide for evaluation of the battery condition in a reasonable time and at the same time small enough to provide no long-term temperature control problem, in case the load could not be disconnected. The 15-W resistor in the propulsion bay was used, which permits assessment in about 30 min.

3. Study to Determine Causes of NAMG Premature Triggering

A study was made in the system design and integration section to determine causes of possible premature triggering of a narrow-angle Mars gate (NAMG). Atmospheric haze, stray light, and other stars and planets were considered as causes.

Since the NAMG-2 output can start the near-encounter flight sequence, a premature triggering of the device

Table 2. *Mariner Mars 1969 spacecraft power margins*

Phase	Gyros	Traveling-wave tube	Power demand, W	Solar panel performance margins, W					
				No flare			Maximum flare		
				Highest	Nominal	Lowest	Highest	Nominal	Lowest
(1) Encounter	off	low	354	191	150	110	98	65	31
(2) Encounter	off	high	390	155	114	74	62	29	-5
(3) Encounter	on	low	391	154	113	73	61	28	-6
(4) Encounter	on	high	427	118	77	37	25	-8	-42
(5) Playback	off	high	330	215	174	134	122	89	55
(6) Playback	on	high	366	179	138	98	86	53	19
(5) Playback[a]	off	high	330	186	148	111	98	67	36
(6) Playback[a]	on	high	366	150	112	75	62	31	0
[a]Applicable if playback lasts up to E + 16 days.									

could mean a loss of some or all of the near-encounter data. It could also increase the problem of running out of digital tape recorder tape before the ultraviolet spectrometer (UVS) and the infrared spectrometer (IRS) have obtained dark-limb calibration data.

The NAMGs are electro-optical devices which consist of light baffles, a lens system, a cadmium sulfide detector, and a trigger circuit which will send a voltage level change to the data automation subsystem (DAS) (from NAMG-2) to initiate the near-encounter sequence and to the pyro subsystem (from NAMG-1) to initiate IRS cooldown and motor start.

The devices have a field of view of 2.5×1.5 deg and, at the nominal triggering time of $E - 15$ min, the projected area of the field of view at the planet limb measures 284×170.5 km. The gates have been designed to trigger on the bright limb of the planet, which has been assumed to have an average brightness of 800 ft-L. The threshold of the trigger circuit was designed to be ⅙ the average Martian brightness, or 133 ft-L. This means that an illumination of 133 ft-L must completely fill the field of view, or ⅙ of the field of view must be filled by the limb of the planet with a brightness of 800 ft-L. Calculations show that the threshold is 0.0485 ft-cd.

Of primary interest in this study is triggering that might be caused by a possible bright atmosphere surrounding Mars. The first picture taken by *Mariner IV* revealed a relatively bright haze in the sky from the limb to the edge of the picture (Ref. 1).

An intensity profile was constructed through this picture on a line perpendicular to the planet limb and through the sky to the furthest corner of the picture. Brightness was assigned based on rectified data numbers furnished by the principal investigator for the television experiment. The data numbers assumed the brightness of a white screen at the Martian distance to be 5300 ft-L. The resulting profile is shown in Fig. 2. An extension of these data was made to the August 1969 period when the brightness of a white screen at Mars was calculated to be 6460 ft-L.
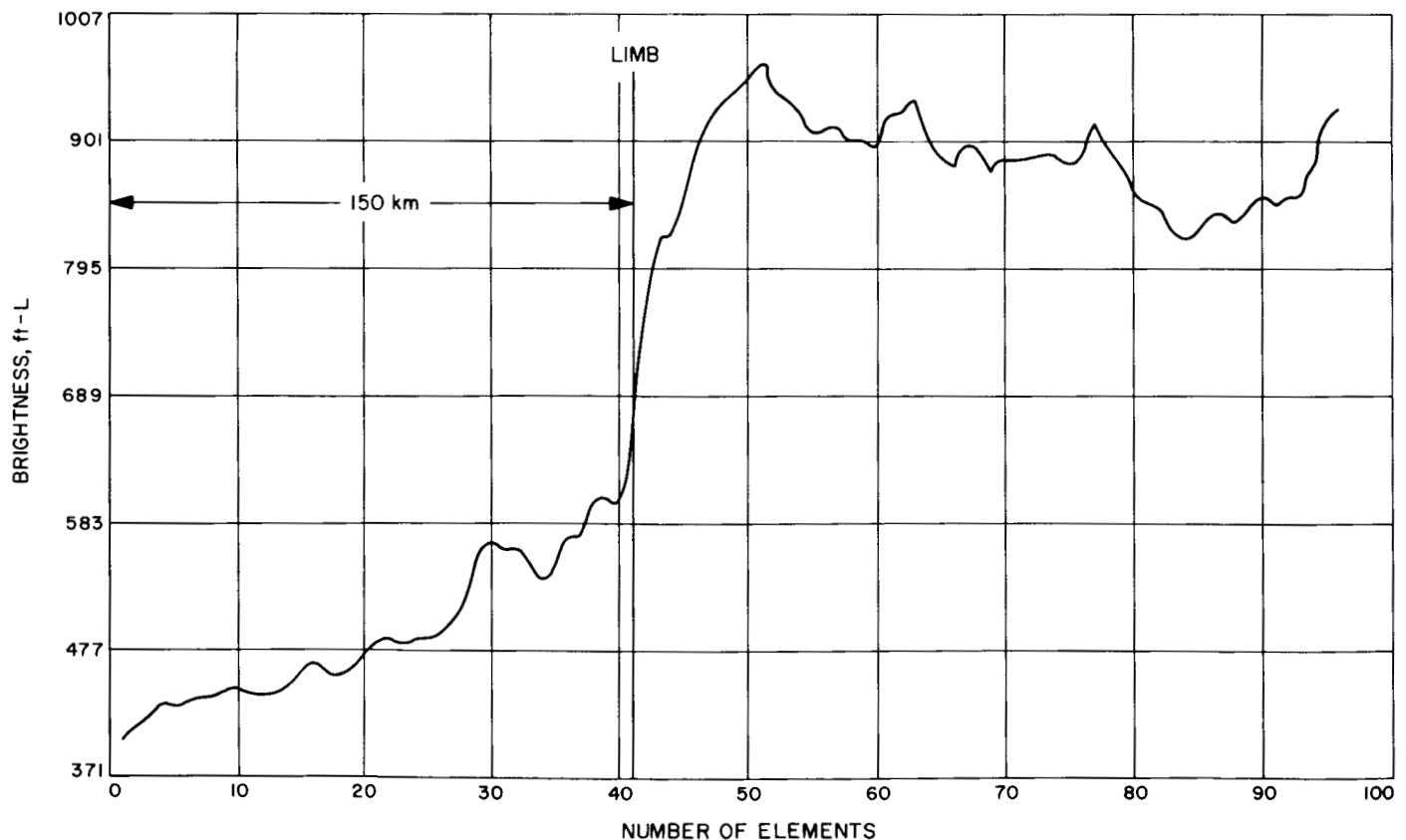

Fig. 2. Brightness intensity profile of first *Mariner* Mars 1964 television picture

Using the relative intensity found in the *Mariner IV* profile, an anticipated brightness profile was made for the August 1969 encounter (Fig. 3). At the furthest edge of the picture from the limb, the sky has a brightness of 497 ft-L when the limb has a brightness on the order of 800–1000 ft-L.

To determine when the NAMG will trigger, as its field of view crosses through the atmosphere to the limb, several assumptions were made:

(1) The edge of the field of view of the NAMG is parallel to the limb of the planet.

(2) The luminous emittance of the atmospheric haze drops off very rapidly at 150 km from the limb (where the *Mariner IV* data end).

(3) The brightness of the atmosphere is constant at equal distances from the limb.

The technique used was to divide the outer atmosphere into layers 7.5 km in depth, starting from the outside edge of the picture. The average brightness of each strip

was then determined. The total energy transmitted to the NAMG was integrated as the field-of-view of the NAMG swept through the atmosphere gathering light from an increasing number of 7.5-km-deep strips or zones.

It was found that after six zones were within the field of view the energy on the detector was sufficient to trigger the NAMG. This amounts to 45 km of the haze within the field of view which corresponds to ¼ of the field of view. If the spacecraft is moving at a velocity of 7 km/s, the NAMG will then trigger approximately 20 s earlier than if triggering occurred at the planet limb without haze.

The stray-light rejection by the NAMG is very good, since its baffle is large compared to the small aperture. It would take a source of 1000 ft-cd located 10 deg off the optical axis to cause triggering. The amount of stray light in the area of the NAMG could be high due to sunlight reflecting off the gas jets at the ends of the solar panels and then off the white surfaces on the under side of the solar panels. However, during the near encounter period when the NAMGs are enabled, their optical axes
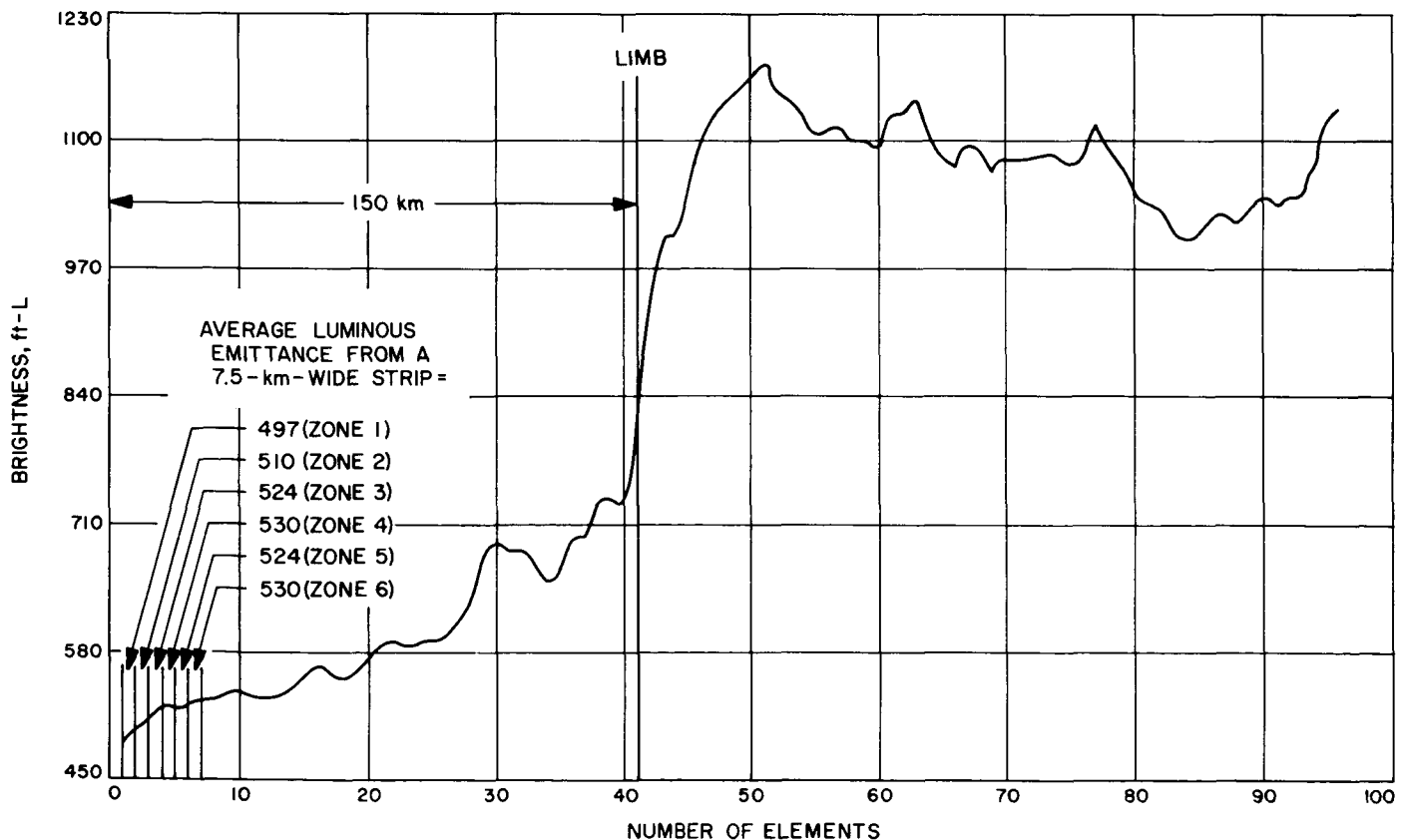

Fig. 3. Predicted brightness intensity profile of *Mariner* Mars 1969 television picture

are at least 50 deg away from the plane of the tips of the solar panels.

The triggering threshold of the NAMG during the encounter period is such that no star, other than the sun, nor any planet, other than Mars, will provide enough light to cause triggering. The sun is excluded from this study, since the other science instruments constrain the boresight axis from ever looking at the sun. The satellites of Mars are very small and will not reflect enough light to cause triggering. They do not even appear in the field of view of the NAMG during the period when triggering will normally occur.

The study has revealed that both NAMGs will trigger approximately 20 s early if atmospheric haze with the same brightness as observed by *Mariner IV* is present out to a distance of 150 km from the limb. Nominal triggering was based on no atmospheric haze.

It would be possible to change the boresight direction of NAMG-2 to lag that of TV so that it would trigger on the bright haze when the TV was pointed toward the limb; however, since the near encounter sequence is also initiated by the TV-PIV (planet in view), the NAMG boresight change would not solve the problem alone.

Premature triggering of NAMG-1 is not as much of a problem as premature triggering of NAMG-2. Twenty seconds is short compared to the total time required for IRS gas-venting cooldown, and the IRS principal investigator has expressed a desire to have the maximum possible cooling timing.

It should be noted that there is a lack of atmospheric brightness data above 150 km; triggering could occur even earlier than predicted in this study if the atmosphere is relatively bright farther out than 150 km.

Reference

1. Allen, J. D., et al., *Mariner Mars 1964 Project Report, Television Experiment, Part I, Investigators' Report*, Technical Report 32-884. Jet Propulsion Laboratory, Pasadena, Calif., Dec. 15, 1967.

4. Spacecraft System Testing and Operations

a. Assembly of M69-1 spacecraft (PTM). Engineering model (e.g., prototype) equipment was removed from the M69-1 spacecraft and replaced with proof-test-model (PTM) subsystem equipment as it became available. By the end of April, M69-1 was completely assembled from PTM equipment, except for one attitude-control gas assembly.

b. Subsystem interface testing. As each engineering model subsystem was replaced with a PTM unit on the M69-1 spacecraft, a subsystem interface test was conducted to: (1) minimize the chance of equipment damage caused by improper interfacing, and (2) functionally test all interfaces between subsystems and verify agreement of their signal characteristics with the values given in the applicable documentation.

c. Subsystem tests. Following verification of the subsystem interfaces, a detailed subsystem test was conducted to: (1) provide a detailed evaluation of subsystem performance during operation on spacecraft power, and (2) allow a preliminary determination of any possible effects the subsystem may have had on the system environment.

d. System test 1. Conducted at the JPL Spacecraft Assembly Facility on March 20–28, system test 1 served to verify the functional performance of the spacecraft as an integrated system within the constraints imposed by the test equipment and the earth-based environment. In general, the problems encountered involved engineering model equipment, and the PTM units performed satisfactorily.

During the test, the spacecraft was exercised in all major elements of a nominal flight sequence. Three different types of trajectory correction maneuvers were performed, as well as two types of far- and near-encounter sequences. Encounter data were played back, using both the normal low-rate capability and the block-coded high-rate (16.2-kbits/s) capability.

e. Power transient survey. A power transient survey was performed on March 28 and 29 to obtain oscilloscope pictures and oscillograph recordings of the power transients produced during the turn-on of the spacecraft subsystems. A secondary objective was to verify that the transients produced were insufficient to cause the spacecraft battery and spacecraft solar panel supplies to go into a sharing mode, even when the total spacecraft power load was at or near maximum. Spacecraft power transients did not cause transfer to the sharing mode.

f. Spacecraft telemetry channel calibration. During early April, spacecraft telemetry channel calibrations were verified and, when necessary, corrected. During the end-to-end calibrations, data were obtained that allowed

verification of computer-derived curves describing the relationship between the data numbers telemetered by the flight telemetry subsystem and the engineering parameter (e.g., voltage, temperature, or pressure) being transduced on the spacecraft.

g. Power profile determination. Preliminary power profile data were obtained in early April to enable an early determination of the power dissipation of each spacecraft subsystem in all of its pertinent steady-state electrical modes of operation. Final power profile data were obtained following the completion of system test 2. These data were used primarily in the development of a spacecraft heat-source profile for performance analysis of the spacecraft temperature-control subsystem.

h. System test 2. In system test 2 performed April 10–18, the functional performance of the spacecraft as an integrated system was verified. Some spacecraft subsystems were not tested to the usual extent for a system test to allow more time for interface problem investigations and detailed evaluation of newly installed PTM subsystems. However, all equipment not installed on the M69-1 spacecraft at the time of system test 1 was thoroughly tested in system test 2.

i. Preliminary scan-control-subsystem telemetry calibration. On April 18, a scan-control-subsystem telemetry calibration was performed to enable a cursory calibration of this subsystem's telemetry data numbers relative to the physical position of the spacecraft scan platform for various sets of far- and near-encounter pointing directions. In addition, the test provided a demonstration of scan-control-subsystem performance, including far-encounter planet sensor control and scan actuator clutch operation.

j. Preparations for space simulation testing. Preparations for the space simulation test in the JPL 10-ft space simulator were made from April 19 to 26. Over 50 instrumentation thermocouples and about 35 auxiliary heaters for spacecraft temperature analysis and control were installed on the spacecraft.

Preliminary spacecraft preparation was performed at the JPL Spacecraft Assembly Facility, while System Test Complex 1 was being installed in the operational-support-equipment area of the Space Simulation Facility. The spacecraft was moved to the 10-ft space simulator and installed on the endbell spacecraft support ring on April 22. Following connection of electrical cabling to the spacecraft, test equipment and spacecraft verification

was performed. Preparation was completed by the successful performance of a spacecraft system verification test designed to verify the proper performance of all spacecraft subsystems.

k. Space simulation test, part I. Part I of the space simulation test was begun April 26 with the evacuation of the 10-ft space simulator. The purpose of part I was to demonstrate long-term (at least 250 h) spacecraft functional performance while operating in a simulated space environment. During part I, the spacecraft was operated through all nominal modes several times while data were compiled for analysis. The nominal simulated space environment was a pressure of less than 5×10^{-5} torr and a cold wall temperature of about $-300°F$.

C. Systems

1. Systems Analysis

a. Specification of LD/AD combinations. During this reporting period, a new plan was formulated for specifying which launch-date/arrival-date (LD/AD) combinations will be targeted. The previous plan consisted of targeting only two fixed ADs selected from the August 1–10, 1969 period. The new, more flexible plan is shown in Fig. 4. Sixty LD/AD combinations have been selected.

The principal investigators are continuing their studies to determine the preferred ADs from July 29 to August 15, 1969. After the completion of these studies (anticipated by early-May 1968), the plan shown in Fig. 4 may be modified as follows: The principal investigators may select 16 new LD/AD combinations, 8 for one currently preferred AD and 8 for the other preferred AD. In addition, they may select up to 10 more LD/AD combinations, if necessary, as long as a corresponding number of cases are eliminated from the 60 cases shown in Fig. 4. Thus, a total of 76 LD/AD cases will be specified for targeting by the launch vehicle system contractor (General Dynamics/Convair).

b. Determination of NAMG setting for IRS sensor cooling. Narrow-angle Mars gate 1 (NAMG-1), located on the scan platform, is used to initiate cooling of the infrared spectrometer (IRS) sensors. It was formerly requested that this sensor initiate cooling (venting of the gas bottles) 15–24 min prior to the time the digital tape recorder starts recording IRS data. Recently, however, the IRS experimenters have requested 18–24 min of cooling time, with the upper end of this range preferred. Resulting from this request and considering such
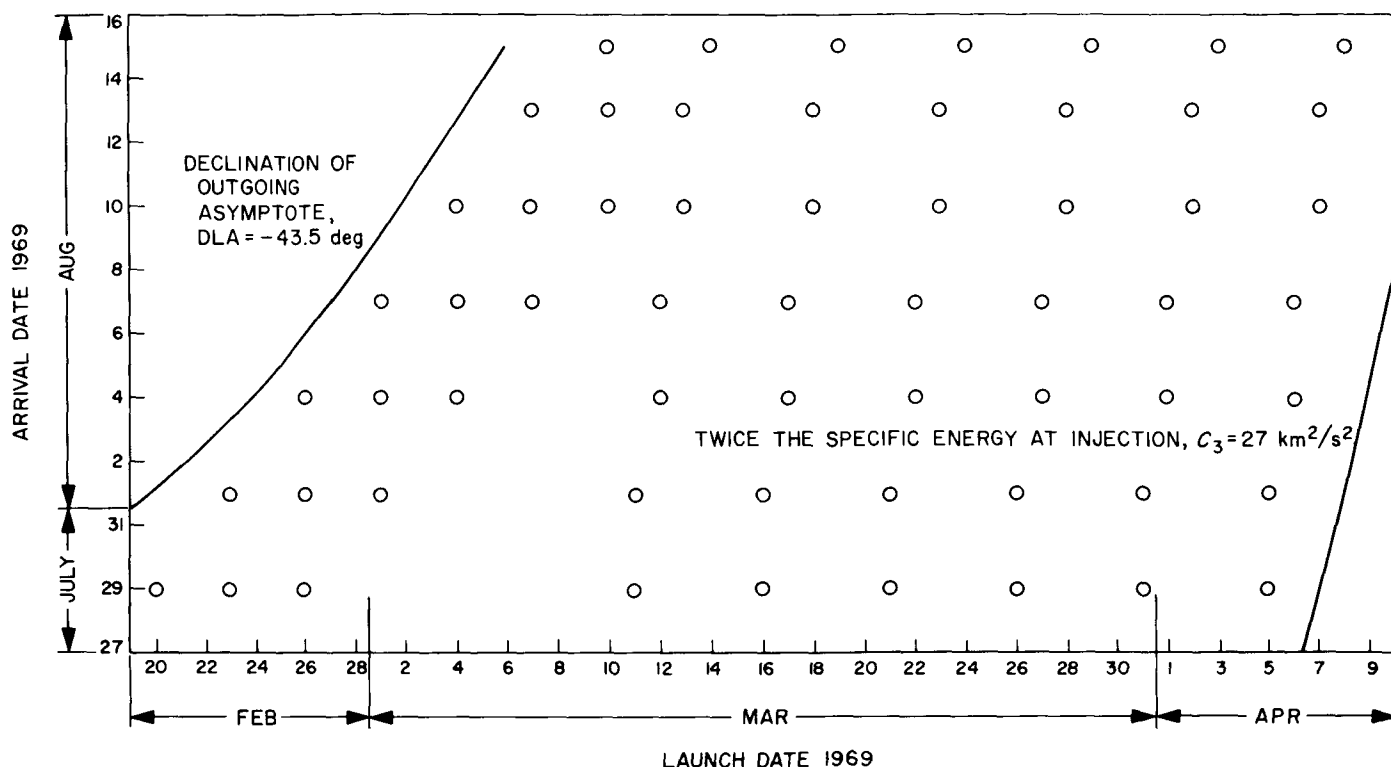
Fig. 4. Specification plan for targeted LD/AD combinations

other "ground-rule" changes as the expanded LD/AD selection plan discussed above, a study was undertaken to determine a new NAMG-1 setting that, for all LD/AD combinations shown in Fig. 4, would provide 18–26 min of IRS cooling prior to start of operation by the digital tape recorder. (The additional 2 min were made available when it was learned that the gas bottles could run for an extra 2 min at regulated pressure.) The study found that no single setting would meet these conditions for all LD/AD combinations; however, a best probable setting of a 34.9-deg Δ cone angle and a −3.1-deg Δ cross-cone angle was recommended. Although this setting fails to satisfy the 18-min minimum precooling requirement for the very late ADs on about August 13–15, more than 16 min were achieved for these cases, and it is felt that the above NAMG-1 setting will be acceptable.

c. Launch-window selection. The recently determined criteria for selecting the location of the 1-h daily firing window are as follows: Consider a plot of launch vehicle excess propellants versus launch time for some LD/AD combination. General Dynamics/Convair, the launch vehicle system contractor, is to select a conservative (based upon such parameters as low *Centaur* performance, and a spacecraft-plus-adapter weight as large as 940 lb) location for the zero excess propellants line

(ZEPL), "excess" propellants being those above the 175-lb flight performance reserve and 100-lb Lewis Research Center contingency. The second crossing of the ZEPL is denoted by t_c. The value 1 h earlier, the launch time, is denoted by t_0. The injection flight path angle for a spacecraft launched at time t_0 is represented by γ_0.

If excess propellants are positive, if $\gamma_0 \leq 10$ deg, and if yaw index, YI ≤ 25, then t_0 is window open and t_c is window close. If YI > 25, t_0 is moved to the right (later in time) until YI $= 25$, and t_c is left as originally defined. If, on the other hand, excess propellants are positive and $\gamma_0 > 10$ deg, General Dynamics/Convair may slide the 1-h window to any new region (earlier in time) beginning at t'_0, providing $\gamma'_0 \geq 10$ deg, YI′ ≤ 25, and excess propellants are still positive. Finally, on those few LD/AD cases where less than 1 h is available, assuming a conservative ZEPL, a more realistic ZEPL will be used to achieve as nearly as possible a 1-h window between the two ZEPL crossings, subject only to the constraint that YI ≤ 25.

d. Targeting specification. Coding of the target specification computer program is expected to be completed during the next reporting period. To generate the actual biased injection aiming-point data and the spacecraft

8

separation and *Centaur* deflection maneuver directions, it was necessary to request injection covariance error and trajectory sensitivity data from General Dynamics/ Convair for the 12 LD/AD combinations (from Fig. 4) representing the 20 cases defined below:

Launch date	Arrival date	Window open	Window close
2/23/69	8/1/69	√	√
3/11/69	8/1/69	√	√
3/26/69	8/1/69	√	√
4/5/69	8/1/69	√	√
3/1/69	8/7/69	√	—
3/12/69	8/7/69	√	—
3/27/69	8/7/69	√	—
4/6/69	8/7/69	√	—
3/10/69	8/15/69	√	√
3/19/69	8/15/69	√	√
3/29/69	8/15/69	√	√
4/8/69	8/15/69	√	√

2. System-Test-Complex Data System

The system-test-complex data system (STCDS) is a computer-based data acquisition and processing system which produces displays of telemetry and hardline data during *Mariner* Mars 1969 spacecraft system tests and science subsystem tests. Its real-time data output consists of: (1) messages on multiple line printers indicating changes in the operating condition of the spacecraft and the operational support equipment, and (2) magnetic tape records of all acquired data. Printouts of the latest available spacecraft subsystem data are available upon request.

The recorded data can be reprocessed by the computer to obtain additional detail, to plot data, or to generate other magnetic tape records in decommutated (frame-synchronized) formats for off-line processing. The principal use of these tapes is to provide the combined science format data (972-bit frame) and television science format data (6804-bit frame) to the image processing laboratory (IPL). These tapes and frame-synchronized tapes containing the real-time science 280-bit frames and the engineering 140-bit frames will also be used as input data sources from which telemetry simulation data will be derived for use in some mission-operations-system/ tracking-and-data-acquisition-system training, engineering, and operational tests. The IPL tapes can also be

produced from recorded, channel C, high-rate, block-coded data and from 18.9-kbit/s analog video data digitized in the science operational support equipment. The block-coded data are decoded by the computer before being recorded on IPL tape. The capability to acquire, process, and format the various types of data for the IPL tapes was fully demonstrated during this reporting period. This capability has proved valuable in various trouble-shooting operations.

Support of the first and second systems tests of the proof-test-model spacecraft was provided during this reporting period. The standard processing capabilities for telemetry as well as events and status data have been developed satisfactorily. Some problems exist in the special processing of science data. Tests of the low-speed analog data system have not yet been completed; the operational-support-equipment interface tests and a hardware/software demonstration remain to be performed. Interface problems have also prevented test and acceptance of the high-speed analog system to be used in the autopilot test. It is still not possible to process and plot the science ultraviolet-spectrometer/infrared-spectrometer 16.2-kbits/s hardline data in real time (SPS 37-50, Vol. I, p. 51). Work is continuing to improve the efficiency of input data buffering, decommutation, and the program executive function to enable this processing.

Following the proof-test-model systems tests, the STCDS data input subsystem and all associated display and control equipment were moved to the space simulator. Immediately after being tested, this equipment began support of a 5-wk proof-test-model test in the space simulator.

Although not anticipated during STCDS design, recent spacecraft testing established conditions of simultaneous launch-mode operation of the central computer and sequencer (CC&S), encounter science data output, and a data storage subsystem data playback. Increased science data acquisition and recording capabilities to support these tests are being provided by using the telemetry input module intended for engineering telemetry support of System Test Complex 2 (Fig. 22, p. 44, in SPS 37-47, Vol. I). By computer selection, it is possible to acquire and record any two of the three low-rate science data streams simultaneously, or all three if CC&S readout is not required. Processing capability is unchanged, and is limited to handling simultaneously one real-time data stream (280-bit frame) and either the flight telemetry subsystem 270-bit/s playback data stream or the data automation subsystem 16.2-kbits/s hardline data.

The second Control Data Corp. (CDC) 3300 computer system is operational. This system includes a set of switches in the computer room which permit switching the test complex display equipment (printers and plotters) and data input subsystem from one computer system to the other for backup in the event of equipment failure. This system is being used for program development, assemblies, non-real-time processing, and some display hardware testing and "debugging" prior to the start of integration with the second data input subsystem in June.

3. Mission Operations

Development of plans for the training and testing of mission operations personnel is continuing. The Mission Operations Training Plan distributed during this reporting period defines the training exercises to be performed by Mission Operations and Tracking and Data System personnel as prerequisites for system tests (to be described in the Space Flight Operations Test Plan scheduled to be issued early in the next reporting period).

A proposal has been approved to provide additional capability to the Phase I simulation program for the Electro-Mechanical Research, Inc. (EMR) 6050 computer in the Space Flight Operations Facility (SFOF). This program with additional data simulation capability, which has been designated Phase IA, will be the prime source of simulated spacecraft data for training and testing operations personnel until proof-test-model spacecraft data are available. Digital magnetic tapes of computer-processed spacecraft telemetry data will be merged into a digital tape with the required mission profile for a particular test exercise. The use of spacecraft data in the digital tape format, rather than the previously planned pulse-code-modulated (PCM) analog tape format, allows the simulation data conversion center (SDCC) to edit and modify the tape information to produce the desired sequence of spacecraft events.

Simulated deep-space-station, automatic-data-switching system, high-speed data line formats and teletype formats will be provided to the SFOF communications interface. A capability will exist to generate PCM magnetic tapes for playback by deep space stations. Also to be provided is a capability to format spacecraft PCM data for real-time transmission to selected deep space stations for processing as normal spacecraft data and subsequent return to the SFOF. The request-for-programming for the Phase IA program is near release, and the preliminary design document is in preparation.

Analog magnetic tape recordings of spacecraft test data are also being produced to serve as a backup data source for the Phase IA program and to be used for simulation of a second spacecraft for some mission operations tests. These analog magnetic tapes will be made on a recorder located in the spacecraft system-test-complex area.

D. Guidance and Control

1. Attitude-Control Subsystem

The attitude-control subsystem requirements of the *Mariner* Mars 1969 spacecraft were very similar to those of the *Mariner* Mars 1964 spacecraft. However, as guidelines for redesigning the subsystem for use on the *Mariner* Mars 1969 spacecraft, it was decided to: (1) substitute improved parts if available and re-evaluate part stress levels to improve reliability, (2) redesign the Canopus sensor to increase the probability of performing automatic roll acquisitions, and (3) incorporate into the Canopus sensor the capability for particle rejection to preclude the possibility of recurring loss of roll reference caused by bright particles in the Canopus sensor field-of-view.

Changes made to the cruise attitude-control subsystem are described below. The final gyro mixing matrix, which is the only item changed for the autopilot subsystem, will be established as soon as final values for the spacecraft moments of inertia, center-of-gravity location, and motor thrust angle are available.

a. Pitch and yaw control

Derived-rate parameters. The derived-rate parameters were re-evaluated using the results of a parametric study. While the *Mariner* Mars 1964 parameters were selected for maximum noise rejection, the *Mariner* Mars 1969 parameters were selected to optimize the spacecraft's ability to recover from disturbing torques. This is a significant change, since it is planned for the *Mariner* Mars 1969 infrared spectrometer subsystem to vent coolant gases during the encounter phases. A comparison of the steady-state position errors for the *Mariner* Mars 1964 and *Mariner* Mars 1969 parameters is given in Fig. 5.

Sun sensor scale factor. The sun sensor scale factor was reduced from 16 to 10.2 V/deg to allow the sun sensors to operate at a lower excitation voltage and thereby significantly improve their reliability.
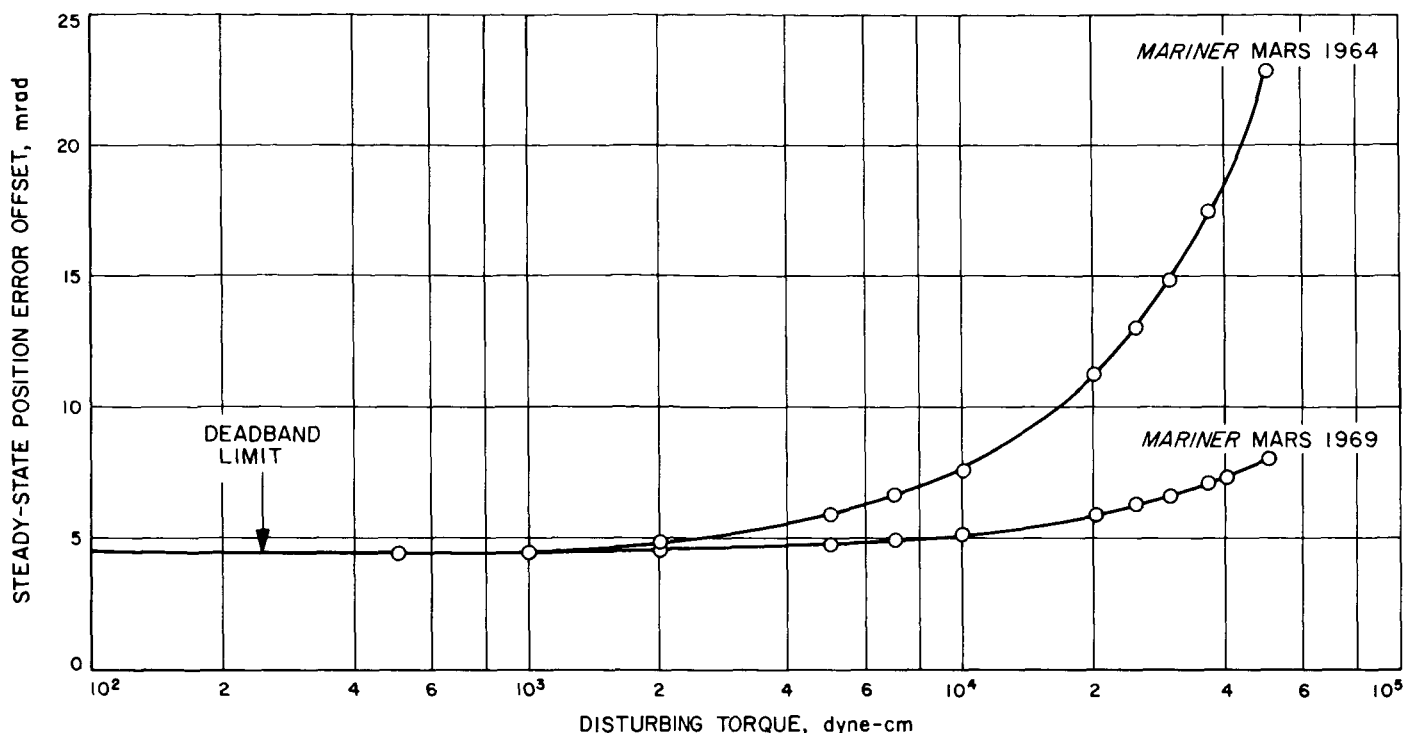
Fig. 5. Steady-state position error offset versus spacecraft disturbing torque

Position deadbands. The pitch- and yaw-axis position deadbands were reduced from ±8 to ±4 mrad to reduce the initial position errors for the midcourse-maneuver turns.

Sun gate and logic. A redundant sun gate design was incorporated. Also, the logic was modified so that a loss of sun acquisition will directly result in the initiation of a sun reacquisition phase. The *Mariner* Mars 1964 logic depended on removing power from the Canopus sensor to initiate a reacquisition phase.

b. Roll control. The changes to the roll axis were of far more significance and scope than those to the pitch and yaw axes. The most significant change was the redesign of the Canopus sensor. The roll control logic was redesigned, and the roll derived-rate parameters were optimized as mentioned previously. The changes to the roll logic are shown in Fig. 6. The general changes to the roll control system are as follows:

Canopus sensor. The new Canopus sensor design utilizes an instantaneous field-of-view (set by tube aperture) of 1 deg, which is electrically scanned to establish a scanned field-of-view of 3 deg. The scanned field-of-view is electronically gimballed to obtain a total field-of-view of 9 deg (roll) by 11 deg (cone). The roll error is generated by observing the position of the scanned field-of-view and the center of the total field-of-view. The scanned field-of-view concept results in improved signal-to-noise performance and allows a larger total field-of-view.

Acquisitions. For acquisitions, whether resulting from no star being in the field-of-view or from a logic command, the scanned field-of-view is biased up against the clockwise edge of the total field-of-view with the following results:

(1) A saturated roll error signal is generated whenever the sensor does not have a star in its total field-of-view. The addition of this signal, which is then used as the roll search generator, allows the deletion of the *Mariner* Mars 1964 roll search generator and simplification of the signal switching.

(2) Reflection problems within the Canopus sensor lens and baffle assembly are eliminated. This deletion of out-of-phase reflection signals during acquisitions allows the deletion of the polarity checking circuitry of the *Mariner* Mars 1964 acquisition logic.

To increase the probability of having an automatic roll acquisition, a scheme utilizing star rejection for both high and low intensity levels has been implemented.
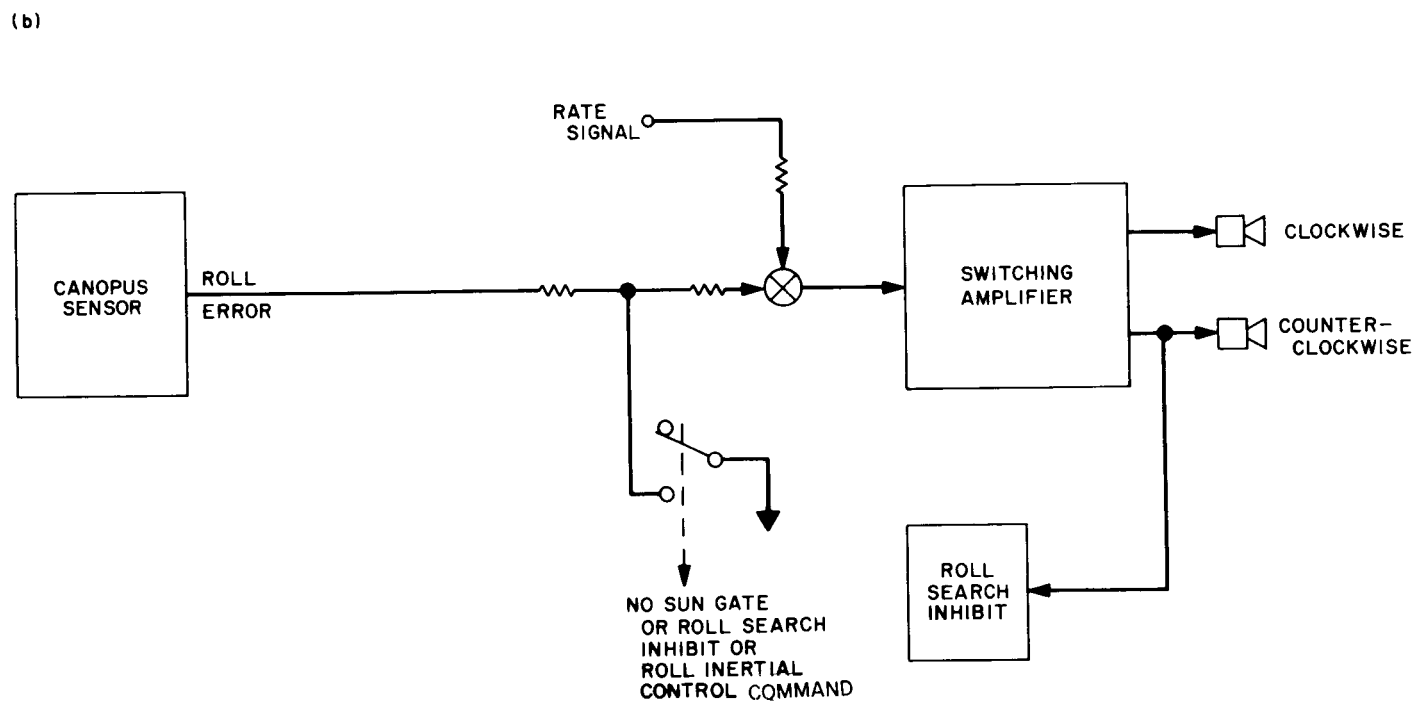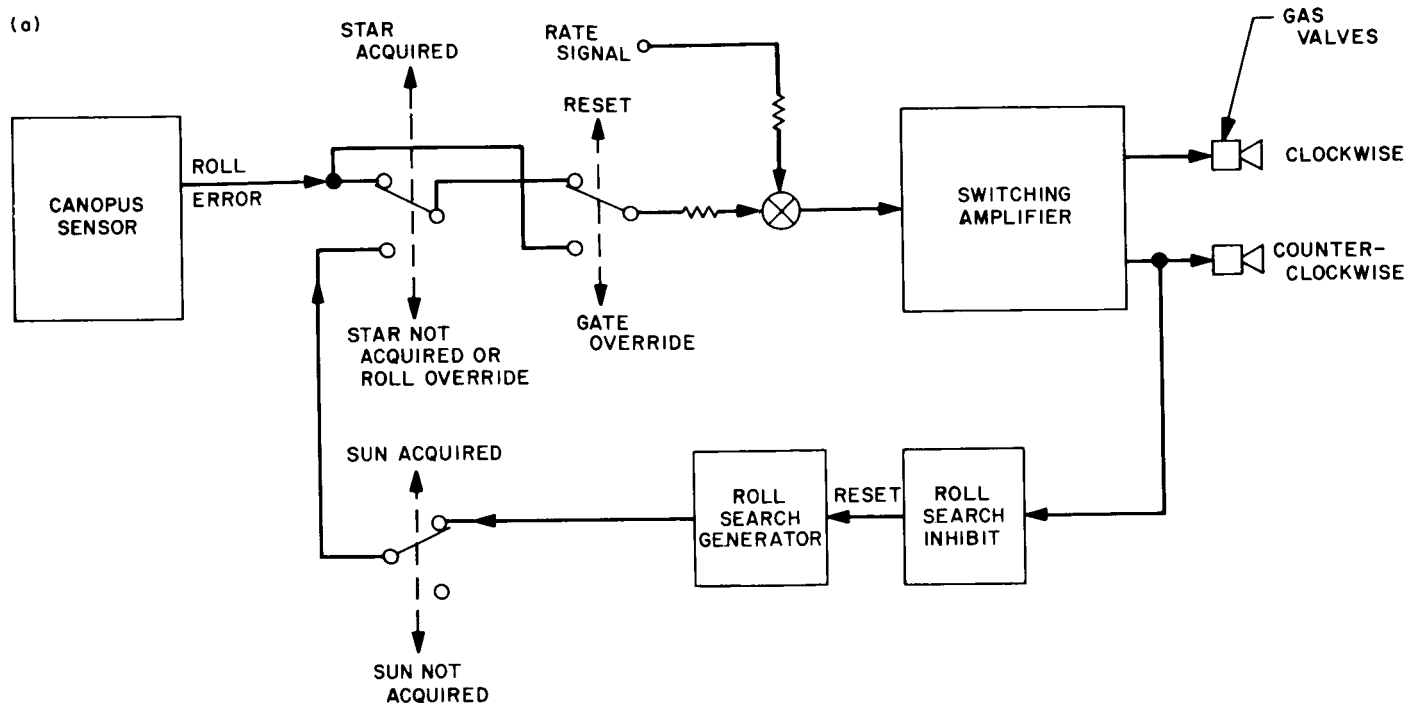
Fig. 6. Roll control logic diagram: (a) *Mariner* **Mars 1964, (b)** *Mariner* **Mars 1969**

The gate setting has been made adjustable in three increments to allow for uncertainties in the calibration of the low intensity gate. This function is cyclic; thus, after the circuit has been stepped to the lowest intensity setting, the next command steps it to the highest. During the actual flight sequence, it is expected that the first intensity level will result in the acquisition of Canopus. However, if due to some unforeseen error the star Canopus does not exceed the first intensity level, the central computer and sequencer cyclic pulse will step the gate to the next level after a minimum of one revolution of roll search. The gate may also be stepped by direct command. The gate settings, normalized to the intensity of Canopus, are 0.8, 0.3, and 0.03 for the first, second, and third gates, respectively.

Particles. To reduce the probability of having a bright fast-moving particle cause the control system to reject a star after acquisition, the following changes were made:

(1) The high intensity gate limit was deleted after acquisition.

(2) A flyback and sweep function along with a time delay was built into the Canopus sensor logic. This will allow a particle to drift through the total field-of-view without causing the spacecraft to go into a roll search until the flyback and sweep function has swept the total field-of-view for the star.

Testing. Both digital computer simulations and breadboard testing have been utilized to verify system compatibility and performance. Breadboard models of the Canopus sensor, the roll control logic, derived-rate networks, the switching amplifier, and the gyro have been assembled into a system and tested in the celestarium. The tests utilized a single-axis table, simulated stars of various intensities, bright Mars and earth disks, and bright-particle simulators. The capability of the system to recover from the effects of external torques and bright particles was verified, as was its capability to acquire a star of Canopus intensity through a search of a bright earth. Results will be published when these tests are repeated with assemblies in final flight configurations.

2. Attitude Reference and Star Identification Programs

To provide the desired support for the *Mariner* Mars 1969 missions [i.e., (1) location and characteristics of various celestial bodies and sources of light relative to the spacecraft for use in preflight analysis, (2) assistance in star identification during flight operations, and (3) data

for post-flight analysis], modifications are being made to the existing Attitude Reference Program for Mariner (ATRM) and Star Identification Program for Mariner (SIPM).

The ATRM modifications are relatively minor, basically providing additional plotting capabilities for parameters generated by the ATRM. The following information will be provided by this program upon request:

(1) Spacecraft coordinates as a function of time from injection.

(2) Clock and cone angles, Canopus ratios, angular diameters, bolometric fluxes, phase angles, and visual magnitudes for Venus, earth, Mars, Jupiter, Saturn, and the moon.

(3) Spacecraft–planet distances.

(4) Sun–planet distances.

(5) Earth–probe–earth communications time.

(6) Bodies (stars, planets, and the moon) in a spacecraft roll window.

(7) Plots of selected parameters from items (2) and (5).

The modified ATRM is scheduled for testing in August.

Major modifications are necessary for the SIPM. Formerly, star identification capabilities were required only during the roll search mode. Logic associated with the *Mariner* Mars 1969 Canopus sensor allows the receipt of telemetry from the sensor during any spacecraft maneuver. Therefore, it will be necessary to provide upon request:

(1) Bodies (stars, planets and the moon) in the field-of-view of the Canopus sensor during any or all spacecraft maneuvers.

(2) Predictions of the Canopus sensor response (in terms of either voltage output or telemetry data numbers) during any or all spacecraft maneuvers.

Testing of the modified SIPM is scheduled to begin in August.

3. Power Subsystem

a. Subsystem testing and modification. The *Mariner* Mars 1969 power subsystem is undergoing tests on the proof-test-model spacecraft at the JPL Spacecraft Assembly Facility. Tests in the thermal-vacuum chamber are scheduled.

Figure 7 is a revised block diagram of the power subsystem (revised from that given in SPS 37-47, Vol. I, p. 51). The approach guidance subsystem has been deleted, and modifications have been made to the relay switching for temperature-control heaters and the output from the Direct Command 50 relay to control the battery test load only. The 15-W test load for the battery will be located on a propulsion fuel tank as a heater load.

b. Power conditioning equipment. Two recent problems in the power conditioning equipment and their solutions were as follows:

Frequency drift in the 2.4-kHz inverter output. The output frequency of the 2.4-kHz inverter, which provides the master clock for the spacecraft, is specified as 2.4 kHz ± 0.24 Hz. However, recent tests at room ambient and 0°C temperatures indicated frequency variations at distinct submultiples of 2.4 kHz.

The frequency drift was caused by noise from the module chassis that was capacitively coupled into the crystal oscillator circuit. The capacitance was that which developed between the chassis plane and the printed circuit board plane. The chassis noise was due to electromagnetic interference coupling of the inverter output stage that caused a noise generator from the 56 Vdc input voltage to return to the chassis.

The inverter output frequency drift was eliminated within a temperature range of -20 to $+90$°C with the introduction of

(1) A ground plane between the chassis and the printed circuit board.

(2) A zener diode to reduce the output impedance of the crystal oscillator buffer.

Kinetics switch. On command from the power operational support equipment, the Kinetics Corp. switch, located in the 4A8 power source logic module, transfers spacecraft operation from the external ground power source to the power source within the spacecraft. The switch recently made such a transfer without command during the type-approval vibration test of the *Mariner* Mars 1969 power conditioning equipment. Data indicate that the transfer was made at frequencies between 1200 and 1600 Hz at a 25-g peak input to the vibration test fixture, and that this input resulted in a peak of 50 g at

the switch case. Several modifications solved the problem:

(1) A more rugged motor that has 5 times the braking torque characteristics of the previous unit will be used to transfer switch contacts.

(2) Vibration characteristics of the switch will be dampened with the use of Solithane[1] mounting pads.

(3) The switch harness will be redressed to improve the switch case dampening characteristics, and Solithane will be used for the wire bond.

c. Battery. The new battery configuration uses an epoxy resin to immobilize the battery plate pack to increase its resistance to vibration damage at launch. Vibration levels to 60 g can be tolerated, whereas the previous battery began to fail at 20 g due to plate shift and wire lead failures. Moreover, negative-plate active material loss from the grid matrix during vibration is reduced with plate immobilization.

However, recent tests on fully charged battery cells have indicated an internal pressure increase at the type-approval ambient temperature of 140°F. Uncured Bondmaster resin used for the plate lock material apparently caused the negative plates to outgas hydrogen, causing the internal battery cell pressure to increase to 50 psig. This pressure was reduced to 30 psig by using modified techniques to process the resin. However, the maximum pressure noted on the *Mariner* Venus 67 cells at similar conditions was 15 psig. Consequently, four batteries will undergo type-approval tests, two of the *Mariner* Mars 1969 configuration and two of the *Mariner* Venus 67 configuration. The first 1969-configuration battery has already been received.

d. Solar array. The *Mariner* Mars 1969 flight solar panels will be built to the exact configuration of the type-approval panel (Fig. 8). The panel array will be fabricated with 17,472 N/P 2- × 2-cm silicon photovoltaic cells and 20-mil fused-silica interference filter coverglasses. Submodules, each consisting of four and five cells connected in parallel by strips of tin-plated Kovar, will be matched into electrical circuits and bonded to four aluminum structures of corrugated design. Each panel, with an area of 20.7 ft^2 and a weight of 26.9 lb, will consist of six isolated electrical circuits, two sections having 780 cells each and four sections having 702
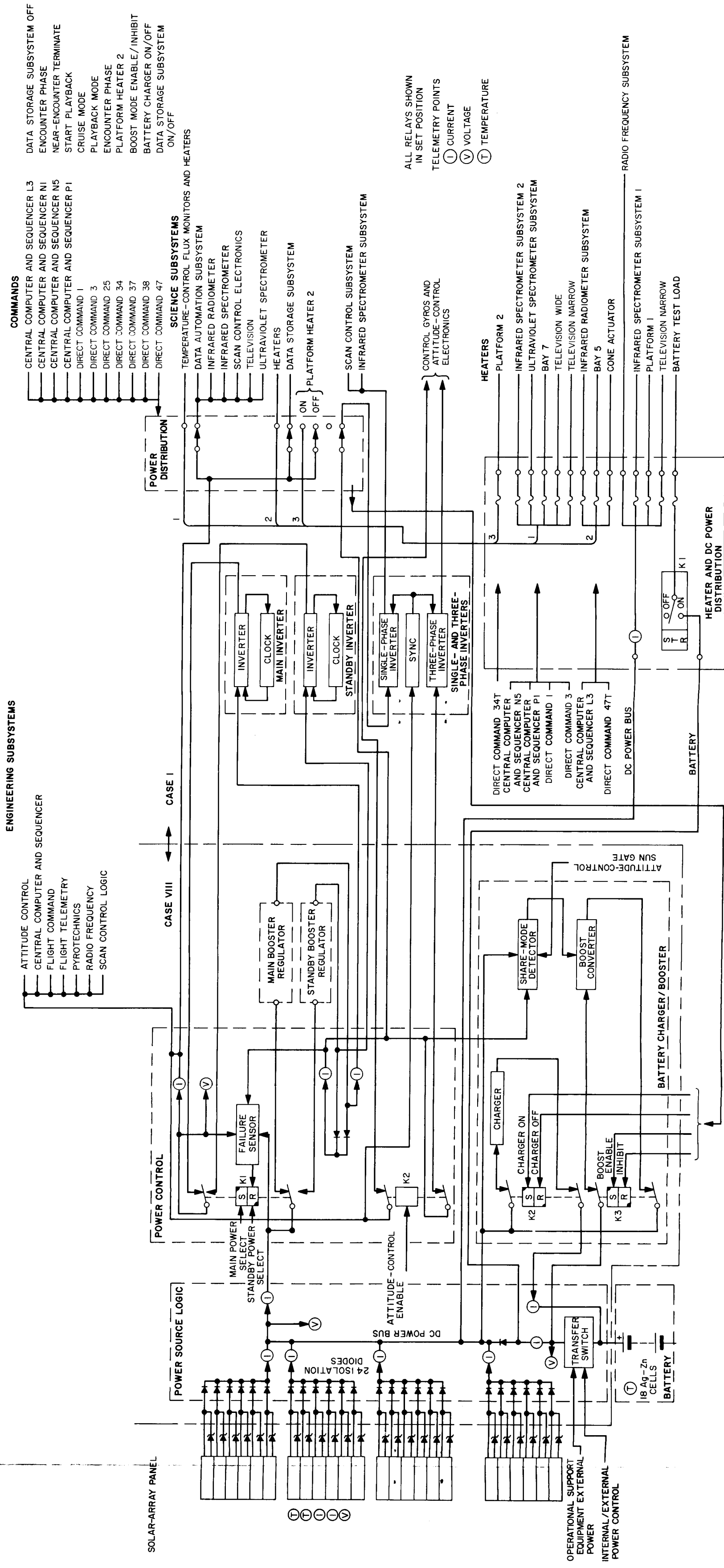
Fig. 7. Power subsystem block diagram (revised)
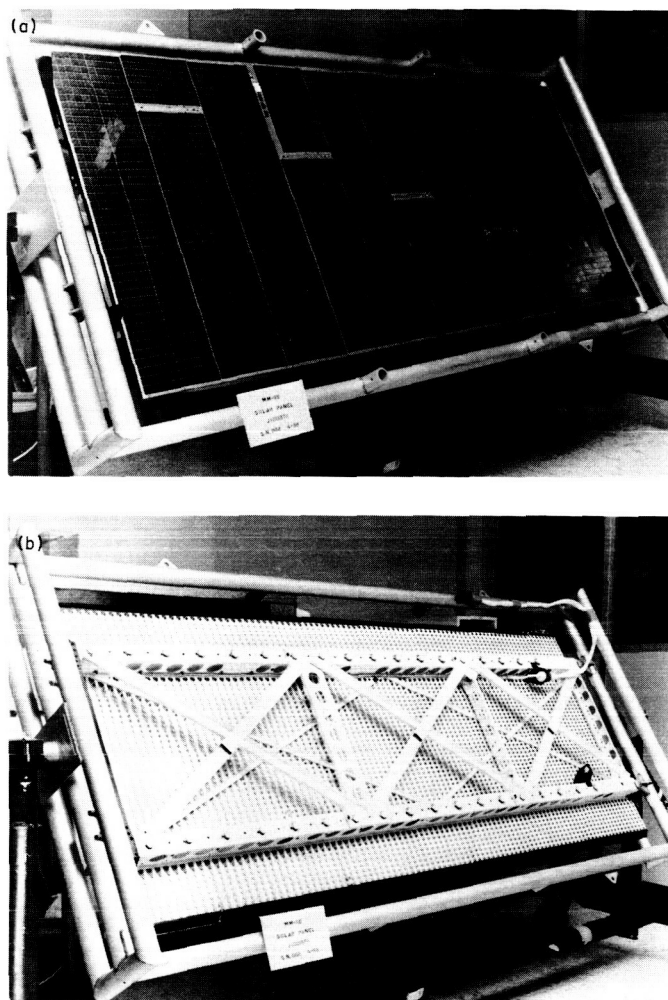
Fig. 8. Type-approval solar panel: (a) front side, (b) back side

Table 3. Electrical outputs of panel extrapolated to nominal undegraded launch and Mars encounter conditions

Circuit	Power, W	Voltage at maximum power, V
Launch conditions		
A	35	31
B	35	31
C	35	31
D	35	31
E	39	31
F	39	31
	Total: 218	Average: 31
Mars encounter conditions		
A	20	39
B	20	40
C	20	40
D	19	39
E	22	39
F	22	40
	Total: 123	Average: 40

cells each. The electrical outputs of the six electrical sections extrapolated to nominal undegraded launch and Mars encounter conditions are given in Table 3.

Type-approval testing has been completed, and the flight hardware program has begun. After each environmental test of the type-approval qualification test series, the solar panel electrical performance was measured at Table Mountain. The qualification tests and the resultant performance are as follows:

(1) *Humidity and vibration.* The panel was placed in the humidity chamber and twice tested for 0.5 h at 38°C and 75% relative humidity. The dynamic characteristics of the panel were then evaluated at flight-acceptance low-frequency and random-noise levels. The electrical output variation after these tests was −1.85%.

(2) *Thermal vacuum.* The panel was tested continuously for 24 h at −55°C and 288 h at 100°C. A −0.15% variation in electrical output was then measured.

(3) *Thermal shock.* The panel was subjected to one thermal cycle starting at ambient temperature, rising to 95°C, lowering to −130°C, rising to 95°C, and lowering to ambient temperature. The maximum shock rates measured from high to low temperatures averaged 38°F/min, and those from low to high temperatures averaged 62°F/min. The measured electrical output variation after this test was −0.76%.

(4) *Acoustic.* The panel was tested to an overall sound-pressure level of 150 dB. An 0.18% variation in output was then measured.

(5) *Vibration.* The dynamic characteristics of the panel corrugations were evaluated at type-approval low-frequency and random-noise levels. The panel was then allowed to electrically operate continuously in sunlight for 8 h. The electrical output variation after these tests was −0.765%.

After the panel was cleaned, a final test showed a 1.20% variation from the initial performance test level.

The electrical output of the panel at the conclusion of the tests indicated the panel had degraded only 1.7%. The successful completion of these tests provided confidence in the solar panel structural design and the compatibility of its parts to the structure.

E. Space Sciences

1. Ultraviolet Spectrometer[2]

The proof test model of the *Mariner* Mars 1969 ultraviolet spectrometer (received March 4) was tested for vibration, shock, explosive atmosphere, and high-vacuum environments. A flexible metallic bellows used as a vacuum seal for a rotary motion transmission device in the optical scanning drive mechanism proved subject to cracking during high-level vibration testing. Changes in materials and wall thickness are being made.

The prototype model of the ultraviolet spectrometer was used during the detailed operational testing of the entire spacecraft system until April 8, when it was replaced by the proof test model.

The flight model 1 spectrometer electronics package was delivered April 15 for integration into the instrument. The finished spectrometer, after its expected delivery to JPL in early-May, will undergo acceptance testing. Delivery of flight model 2 and 3 subassemblies is also expected in May.

2. Infrared Spectrometer[3]

The prototype infrared spectrometer was used to support proof-test-model spacecraft testing prior to delivery of the proof-test-model instrument. The prototype was then returned to the University of California, Berkeley in mid-April for incorporation of the approved design modifications. An auxiliary gas delivery system was installed at the JPL Spacecraft Assembly Facility to allow the instrument cryostat to reach operational temperature (22°K), thus providing more complete instrument performance verification through spectral measurements of an external stimulus.

As a result of numerous failures during initial calibrations and type-approval testing of the monochromator–telescope assembly, several minor design and procedural changes were made. Following limited additional testing

for verification purposes, the instrument was delivered to the JPL Spacecraft Assembly Facility in mid-April, where it operated satisfactorily during system-level testing.

The fabrication of the first flight model is complete, and fabrication of the second and third flight models is progressing.

3. Infrared Radiometer[4]

The thermal-vacuum portion of the type-approval tests was conducted on the proof-test-model infrared radiometer from March 8 to 21 with no problems occurring. During tests to revised project vibration levels on March 22, the motor shaft fractured during the sine-wave down sweep on the spacecraft X-axis. It was later determined that the increased g-level requirements coupled with the amplification factor through the radiometer had resulted in the motor shaft design limits being exceeded. The motor shaft has since been redesigned.

The radiometer, mounted on the proof-test-model spacecraft on April 9, successfully completed systems tests conducted on that vehicle the following 2 days.

The flight model 1 radiometer has been fabricated and is presently in the checkout phase at the Santa Barbara Research Center. Flight-acceptance testing at JPL is scheduled to begin April 25. Fabrication of the flight model 2 and 3 radiometers is progressing; delivery is expected in May.

4. Data Automation Subsystem[5]

The prototype, the proof test model, and flight models 1, 2, and 3 of the data automation subsystem (DAS) have been delivered, as has all hardware for the bench checkout equipment. The prototype has been used in support of the operational support equipment 2 science system integration effort and the DAS programmed data processor 7 (PDP-7) checkout. The PDP-7 checkout system includes a computer and interface rack. A DAS is required since the system's operation is not simulated.

The DAS proof test model has successfully met type-approval requirements and has operated with voltage variations of −15 to +40% of the nominal operating voltage. During this reporting period, the proof test

---

[2]General description given in SPS 37-47, Vol. I, p. 66.

[3]General description given in SPS 37-47, Vol. I, p. 66; photographs included in SPS 37-50, Vol. I, pp. 83 and 84.

[4]General description given in SPS 37-47, Vol. I, p. 71; photographs included in SPS 37-50, Vol. I, p. 85.

[5]Description given in SPS 37-49, Vol. I, pp. 24 and 25.

model was used in support of spacecraft systems integration and two complete system tests. Its compatibility with all interfacing subsystems and its reliability have been proven.

Flight models 1 and 2 met flight-acceptance test requirements. The flight model 1 life test under vacuum was begun March 25. Flight model 2 began a life test at −10°C on April 15.

The breadboard has been used in support of the operational support equipment 2 and PDP-7 checkout and as a test bed for all engineering changes.

The First Article[6] life test was started in mid-January and has run 2150 h as of April 16. For this test, 253

---
[6]One tray with representative mechanical and electrical elements.

integrated circuits are being tested at temperatures from −55 to +125°C.

The "control board," that has been fabricated to provide information for investigating the problem of the cracked integrated circuit case, has completed the final stages of environmental testing at JPL. Electrical tests under thermal-vacuum conditions are to be continued at Litton Systems, Inc. (the manufacturer of the DAS) for approximately 10 mo. The control board will be inspected periodically for additional cracked cases and/or increase in the severity of existing cracks to help determine if the problem is dependent on time. No additional cracks have yet been found.

The type-approval, flight-acceptance, and systems tests conducted thus far have established a high level of confidence in the design and manufacture of the DAS.

II. Surveyor Project

LUNAR PROGRAM

A. Introduction

The objective of the *Surveyor* Project was to soft-land a series of spacecraft on the moon to obtain information to support the *Apollo* Project. Seven missions were planned. *Surveyors I, III, V,* and *VI* successfully met the objective of the project; each landed at a site within the proposed *Apollo* landing zone, an area bounded by ±45° lon and ±5° lat; specifically, the landing sites were those given in Table 1.

Table 1. Surveyor spacecraft landing sites

Spacecraft	Launch date	Landing site
Surveyor I	5/30/66	Relatively flat, smooth surface encircled by hills and low mountains in Oceanus Procellarum
Surveyor III	4/17/67	Inner wall (at 14-deg tilt), halfway between center and rim crest, of a subdued, medium-sized crater in Oceanus Procellarum
Surveyor V	9/8/67	Inner wall (at 20-deg tilt) of a small, rimless crater in Mare Tranquillitatis
Surveyor VI	11/7/67	Flat surface of Sinus Medii near a mare ridge

Due to the previous successes, *Surveyor VII*, launched 1/6/68, was designated primarily a science mission. The landing site was the ejecta blanket north of the crater Tycho. This site was selected since Tycho is the youngest crater that was accessible to the *Surveyor* spacecraft, and it is assumed that its ejecta are the least contaminated.

The successful photogrammetric experiments with the television camera carried on all the *Surveyor* spacecraft proved the value of the camera as a scientific instrument. Over 85,000 photographs were received from *Surveyors I, III, V, VI,* and *VII,* some of which are stereoscopic and some in reconstituted color. The photographic evidence has, to a large degree, confirmed estimates made from earth-based observations concerning the detailed configuration of the lunar surface.

In addition to photographing the lunar surface, the television cameras were also used in many successful spatial experiments, including:

(1) Photographing earth from another celestial body (performed by *Surveyor III*).

(2) Photographing a total eclipse of the sun by the earth (performed by *Surveyor III*).

(3) Photographing the solar corona from another celestial body (performed by *Surveyor I*).

(4) Photographing light signals aimed at the spacecraft from earth during the *Surveyor VII* laser experiment.

(5) Photographing stars (Sirius, Canopus, Vega, and some minors), planets (Jupiter, Venus, and Mercury), and constellations (Gemini and Orion) from outside the earth's atmosphere.

Soil mechanics experiments, employing a remotely commanded surface sampler with a scoop in conjunction with the television camera, were performed by *Surveyors III* and *VII*. Operations included bearing tests of the lunar surface with the scoop both open and closed, trenching operations, impact tests, and an experiment to shear off a fragment from a rock. The lunar soil, made up of fine, granular material, was found to be weakly cohesive, behaving like fine, damp soil on earth. The surface-sampler scoop also participated in the first successful attempt of a spacecraft to correct its own mechanical malfunction; for this operation, the scoop exerted pressure on the *Surveyor VII* alpha scattering instrument head to force it to the lunar surface after that instrument's lowering mechanism malfunctioned. This instrument's head was also repositioned onto other locations on the lunar surface by the scoop.

Surveyors V, VI, and *VII* carried on alpha scattering instrument that could detect the presence of a wide range of chemical elements. The results of this experiment indicate that the overall composition of the lunar soil examined is basaltic in character and that the elements present in the surface material are in the form of oxides and comprise compounds and minerals well-known on earth.

A magnet experiment was also performed by *Surveyors V, VI,* and *VII*. This experiment was passive in that it required no special electronics, it was not a commandable operation, and its results had to be viewed by the television camera. For the experiment, a magnetic bar and a nonmagnetic control bar were attached to a foot-pad on *Surveyors V, VI,* and *VII*. Horseshoe-shaped magnets were also imbedded in the soil mechanics/surface sampler scoop door on *Surveyor VII*. Comparison of the magnet experiment data with laboratory data suggests a low magnetic-particle content. These results are consistent with a basaltic composition having little, if any, meteoritic iron addition.

This issue of the SPS, Vol. I, will be the last to include *Surveyor* Project reporting.

B. Space Sciences

1. Near-Real-Time Ground Data Processing System for Alpha-Scattering Experiment

a. Alpha-scattering experiment data processing requirements. The alpha scattering instrument on *Surveyors V, VI,* and *VII* (Refs. 1–5) was designed to measure the elemental composition (in at. %) of the top layer of the lunar surface. The lunar surface was bombarded by monoenergetic alpha particles emitted from six collimated sources of curium 242 located in the instrument head, deployed to the lunar surface. The energies of both back-scattered alpha particles and protons generated from the (α,p) reaction in the lunar surface were measured separately by two alpha and four proton solid-state detectors in the instrument head. These energies were separated into a spectrum of 128 channels in an analog-to-digital converter, and the alpha and proton spectral information was sent to earth using separate transmission channels. Both the alpha and the proton spectra were characteristic of the nuclei of the elements with which the alpha particles interacted, and the contribution of each atomic species to the scattering could be considered additive.

Because of weight restrictions on the instrument, it was planned that the outputs of the two alpha and four proton detectors would be separately summed into two data streams early in the spacecraft signal processing. With such summing of data, a malfunction in a detector would influence the total output of the data stream generated by that type of detector. A slight detector malfunction would reduce the analytical accuracy of the data, and a serious malfunction could render the data useless.

However, a capability was incorporated to remove, by earth command, any combination of detectors from the counting operation. Thus, if a detector malfunction could be traced to a specific detector, it was possible to isolate that detector and incur no data degradation. The necessity for the isolation of malfunctioning detectors was a major factor leading to the implementation of a near-real-time ground data processing system for this experiment.

A second reason for near-real-time processing concerned the irreversible sequence of events leading to the deployment of the instrument head to the lunar surface.

Before deployment occurred, it was necessary that sufficient good data be available to accurately assess both lunar background radiation and the performance of the instrument while in contact with a known standard sample.

b. System description and performance. In the ground data handling system (Fig. 1), data processing took place at the three deep space stations (DSS) supporting the alpha scattering experiment (Pioneer DSS, California; Robledo DSS, Spain; and Tidbinbilla DSS, Australia) and at the JPL Space Flight Operations Facility (SFOF), where the experiment was controlled.

DSS data processing. Each DSS system was configured as shown in Fig. 2. For the real-time operations, the alpha and proton data streams were demodulated, discriminated, and conditioned to be acceptable to a Scientific Data Systems (SDS) 920 computer. The two incoming data streams were bit synchronized and blocked into data words representing the energies of the detected alpha particles and protons. The channel number of each word was determined, and its parity was checked. (On the spacecraft, the alpha and proton energies were encoded by the instrument electronics into 9-bit data words: 1 sync bit, 7 information bits, and 1 parity bit.)
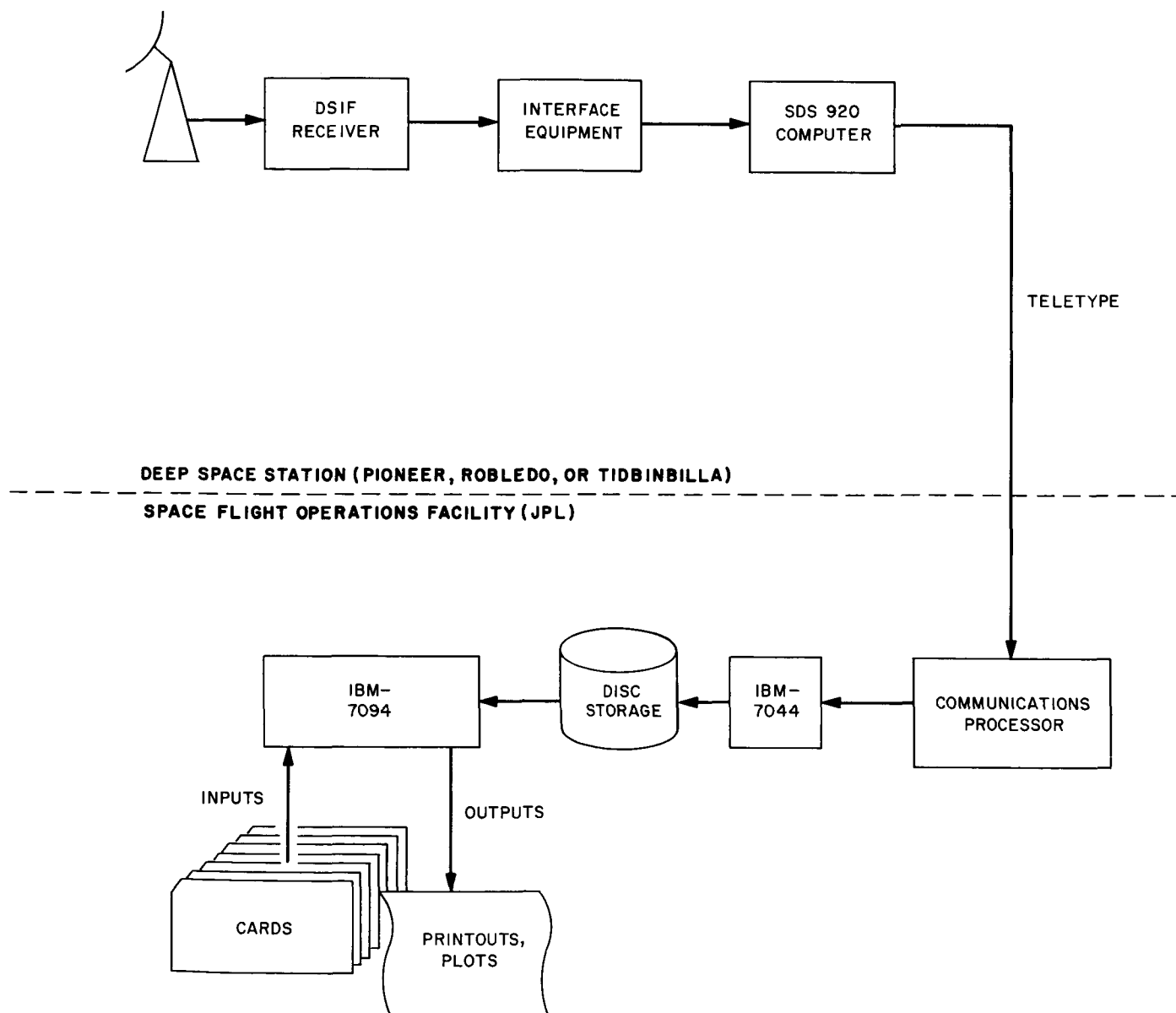

Fig. 1. Ground data processing system for alpha scattering experiment
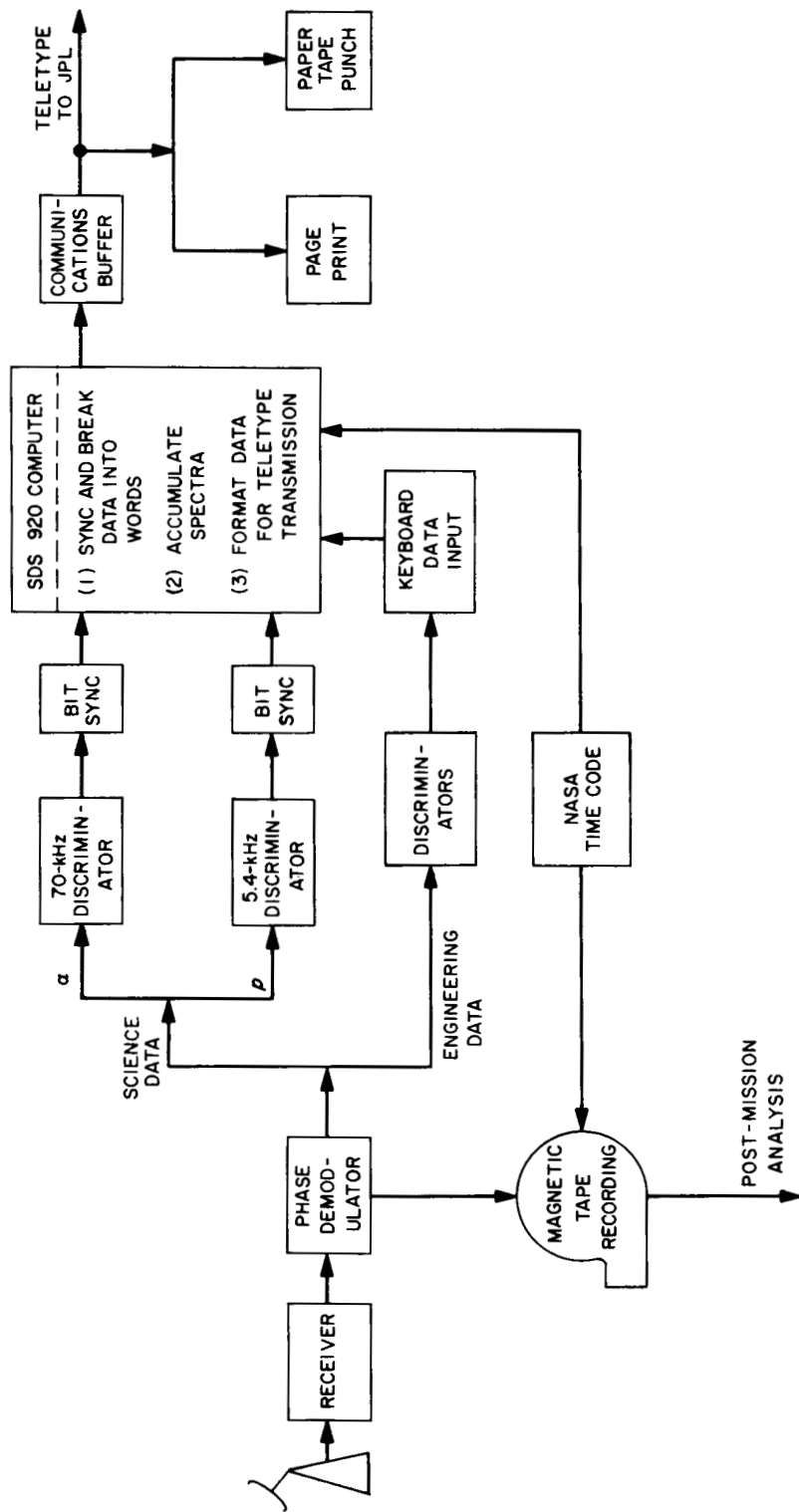
Fig. 2. DSS data processing system

Upon external keyboard command, four spectra representing the number of events detected in a given energy channel (alpha, proton, alpha-parity-incorrect, and proton-parity-incorrect conditions) were simultaneously accumulated. During the accumulation, it was possible by keyboard command to interrogate the computer for the current status of any channel in any spectrum. This feature permitted gross assessment of detector performance with a much shorter reaction time than was possible transmitting a full-length accumulation. Also upon keyboard command, a given accumulation was stopped and the four spectra, as well as other identifiers, were transferred to magnetic tape and/or teletype lines for periodic transmission to the SFOF.

The primary function of the on-site processing was the substantial data compression that enabled this transmission. Typical spectral accumulations of lunar surface data lasted 20 to 40 min, with a constant transmission time for each accumulation of approximately 10 min. The number of accumulations for each of the *Surveyor* alpha scattering experiments is as follows:

Mission	Number of accumulations	Total time, h
Surveyor V	394	108
Surveyor VI	282	62
Surveyor VII	361	105

It should be noted, however, that the total times listed above include some redundant data accumulated when two DSSs were receiving data simultaneously, 14 h of data for *Surveyor VI* when the instrument head was overturned, and calibration data. Therefore, they should not be considered as exact figures for the amount of data received from the instrument.

For post-mission analysis, the composite signals received from the spacecraft were demodulated and then recorded in analog form on magnetic tapes. These analog tapes were later processed at JPL using a UNIVAC 1219 computer. The relevant alpha scattering data were transferred to digital magnetic tapes for analysis by the principal investigator (Prof. A. Turkevich, University of Chicago).

Each DSS system performed satisfactorily, with relatively few data accumulations lost by equipment malfunctions or operator errors. It should be emphasized that this small data loss affected only the real-time operations, since all data were recorded separately for post-mission analysis.

SFOF data processing. The batches of raw spectra data were further processed at the SFOF to permit a detailed analysis of instrument behavior and to provide preliminary compositional analyses of the lunar surface. These processing operations, using a coupled IBM 7044/IBM 7094 system, are shown in Fig. 3. At each stage of the processing operations shown, the data were plotted using an off-line Stromberg Carlson 4020 plotter.

A modular program design permitted considerable operational flexibility; e.g., by card input the modules could be run in any order, skipping or repeating any modules desired. This flexibility enabled calculations other than those originally planned.

After encoding by the IBM 7044, the teletype data were automatically recorded on disc for use by the IBM 7094. Data could also be entered into the system by cards from the operations area. This feature proved particularly valuable, since it permitted reanalyzing certain data to assess the effects on the results of changing the processing parameters.

Particular attention was directed in program design to the problem of automatically handling input data that contained spacecraft-to-DSS and DSS-to-SFOF transmission errors. A line-by-line searching scheme proved extremely effective, even with data containing many errors. However, the great majority of the teletype data were free of significant errors.

The initial step in the computer processing involved correcting the transmission errors, using the parity checks included in each transmission. Parity violations were automatically flagged by the computer, and corrections were made either automatically using linear interpolation or through manual editing by card input.

As the temperatures of the alpha scattering instrument electronics and sensor head changed, the relationship between channel number and detected particle energy also changed. The second stage in computer processing automatically realigned the channel numbers, using values of temperature included in the teletype transmission; thus, any given channel number always corresponded to the same particle energy interval. In this way, it was possible to consistently combine spectral accumulations in terms of a channel-by-channel addition. The correction parameters used for the energy scale realignment (as well as most other program parameters) were changed in real time through card inputs from the

DISC STORAGE

EDIT DATA

DETECT/CORRECT FOR
DSS-TO-SFOF
TRANSMISSION ERRORS

PRINTOUT
FLAGGED
PARITY
ERRORS

CORRECT FOR 2-BIT
TRANSMISSION ERRORS
IN SPACECRAFT-TO-EARTH LINK

PRINTOUT
CORRECTED
SPECTRA

CORRECTION
PARAMETERS

CORRECT FOR ENERGY SCALE
SHIFTS IN THE ALPHA
SCATTERING INSTRUMENT

PRINTOUT/PLOT
CORRECTED
SPECTRA

BATCHES/
BACKGROUND TO
BE INCLUDED

SPECTRAL SUMMING

PRINTOUT/PLOT
SUMMED
SPECTRA

SPECTRAL
LIBRARY
TAPE

ELEMENTS TO
BE INCLUDED
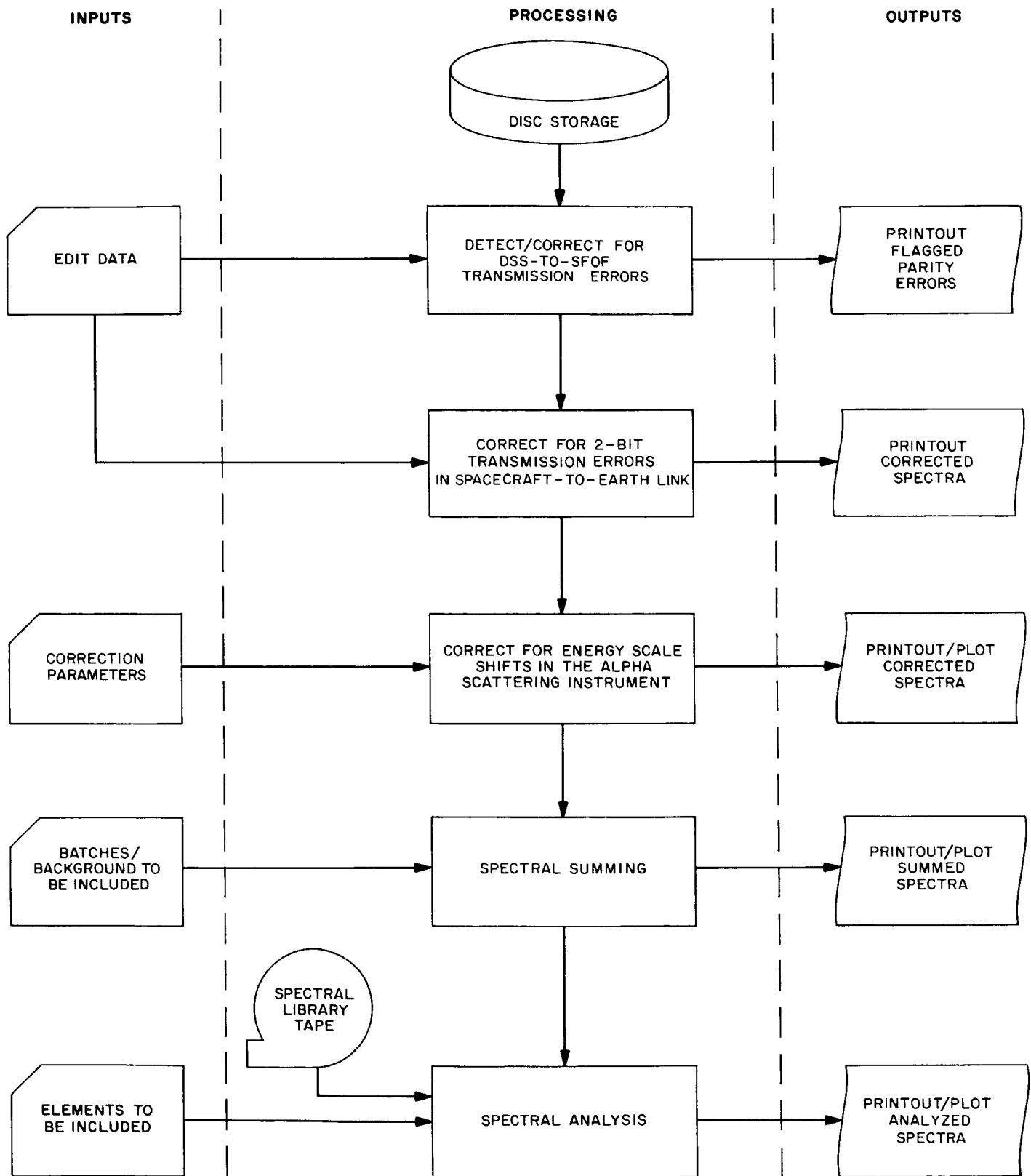
SPECTRAL ANALYSIS

PRINTOUT/PLOT
ANALYZED
SPECTRA

Fig. 3. SFOF data processing operations

remote user area. After transmission and energy corrections were applied, each spectral accumulation was stored on magnetic tape for further processing.

Each incremental accumulation of data represented the spectral results from a period of nominally 30 min. To produce a more statistically reliable spectrum, many accumulations were summed, forming a single alpha and proton spectrum. This was done by entering the desired identifying indices for the batches to be summed, as well as indicating an appropriate background (either measured or theoretical) to be subtracted from the sum. Not only was a more statistically meaningful result achieved, but anomalous instrument behavior could be detected by spectral changes resulting from the incorporation of a new spectral batch.

The measured alpha and proton spectra were the result of scattering from the nuclei of the elements making up the lunar surface. The elemental composition of this surface layer could be determined by finding that combination of elements which yielded the "best fit" to the observed spectra. This was performed in the final stage of the processing, when the corrected and summed spectra were fit to a previously prepared library tape of elemental spectra, using a weighted least-squares regression procedure. The weighting factor used in this fit was the reciprocal of the estimated variance in each channel.

In the least-squares fit, three different spectra were treated: (1) a selected range of channels in the alpha spectrum only, (2) a selected range of channels in the proton spectrum only, and (3) the "spectrum" obtained by considering both the alpha and proton spectra as a single spectrum. Any significant degradation in the "goodness of fit" when a new batch was added to a previously analyzed sum was an indication that anomalous instrument behavior had occurred.

The alpha scattering instrument also contained an internal electronic pulser which would, on earth command, introduce two sharp peaks into each spectrum to serve as a calibration of the instrument electronics. This mode of operation was also handled automatically by the ground data processing system. No changes to accommodate it were required in the DSS processing; however, the data were automatically treated in a different manner in the SFOF processing. After transmission corrections were applied, the peak positions and half-widths were determined, and relevant calibration parameters were calculated.

The SFOF computer program performed very well during mission operations, analyzing virtually all data received by teletype in near-real time. The information contained on the digital magnetic tapes for the post-mission analyses appears to agree well with that obtained from the near-real-time system.

References

1. Patterson, J. H., Turkevich, A. L., and Franzgrote, E., "Chemical Analysis of Surfaces Using Alpha Particles," *J. Geophys. Res.*, Vol. 70, p. 1311, 1965.

2. Turkevich, A. L., et al., "Instrument for Lunar Surface Chemical Analysis," *Rev. Sci. Instr.*, Vol. 37, p. 1681, 1966.

3. Turkevich, A. L., et al., "Chemical Analysis Experiment for the Surveyor Lunar Mission," *J. Geophys. Res.*, Vol. 72, p. 831, 1967.

4. Turkevich, A. L., Franzgrote, E., and Patterson, J. H., "Chemical Analysis of the Moon at Surveyor 5 Landing Site," *Science*, Vol. 158, pp. 635–637, 1967.

5. Turkevich, A. L., Patterson, J. H., and Franzgrote, E. J., "Chemical Analysis of the Moon at the Surveyor VI Landing Site: Preliminary Results," *Science*, Vol. 160, pp. 1108–1110, 1968.

2. Chemical Analysis of the Lunar Surface at the Surveyor V, VI, and VII Landing Sites

The first chemical analyses of lunar surface material were obtained by means of the *Surveyor* alpha scattering experiment in Mare Tranquillitatis and Sinus Medii (equatorial mare landing sites of *Surveyors V* and *VI*, respectively) and in a terra region near the crater Tycho (landing site of *Surveyor VII*). Preliminary results are reported in Refs. 1–3.

The chemical composition of the first sample examined at each of the three sites is given in Table 2. Two samples were examined at the *Surveyor V* site and one at the *Surveyor VI* site. Since the surface sampler was used to move the alpha scattering instrument on *Surveyor VII*, data were obtained from three positions on the lunar surface, each position representing a different type of local sample: undisturbed surface material, a lunar rock, and an extensively trenched area.

The three most abundant elements found at the *Surveyor V* site (Ref. 1) are the same as those in the crust of the earth, namely: oxygen, silicon, and aluminum, with abundance decreasing in that order. The results indicate that the sample analyzed is a silicate similar to materials available on earth. Of several comparisons with such materials, the closest agreement appears to be with the chemical compositions of basaltic achondrites and terrestrial basalts.

Table 2. Chemical composition of the lunar surface at the Surveyor V, VI, and VII landing sites: preliminary results

Element	Abundance,[a] at.%		
	Surveyor V	Surveyor VI	Surveyor VII
Carbon	<3	<2	<2
Oxygen	58 ±5	57 ±5	58 ±5
Sodium	<2	<2	<3
Magnesium	3 ±3	3 ±3	4 ±3
Aluminum	6.5 ±2	6.5 ±2	8 ±3
Silicon	18.5 ±3	22 ±4	18 ±4
"Calcium"[b] ⎫ ⎬	13±3[d]	⎧ 6 ±2	6 ±2
"Iron"[c] ⎭		⎩ 5 ±2	2 ±1

[a]Excluding elements lighter than beryllium.
[b]"Calcium" here denotes elements with mass numbers between approximately 30 and 47 (e.g., phosphorus, sulfur, potassium, and calcium).
[c]"Iron" here denotes elements with mass numbers between approximately 47 and 65 (e.g., chromium, cobalt, nickel, and iron).
[d]Result for the total of elements heavier than silicon. A lower limit of 3% was set for "iron."

The chemical composition of the lunar surface material sampled by *Surveyor VI* in Sinus Medii is very similar to that of the surface material sampled by *Surveyor V* in Mare Tranquillitatis. This agreement provides a basis for assuming that considerable portions of the mare areas of the moon have a similar composition. This similarity of results from the two missions is demonstrated by the detailed results of computer analysis of the data presented in Table 2. A direct comparison of the raw spectra from the two mare sites also indicates very good correlation between the *Surveyor V* and *VI* results (Ref. 2).

In general, the composition of the undisturbed surface material sampled by *Surveyor VII* is not significantly different from that of the surface material sampled by *Surveyors V* and *VI*. There is no doubt, however, that the abundance of the "iron" group of elements at the terra site is significantly lower (by about a factor of two) than that at the mare sites. This difference has been confirmed by examination of the raw data from the experiment (Ref. 3). Data from the other samples (lunar rock and extensively trenched area) support these findings.

Although only part of the data has been analyzed thus far, and that only in a preliminary manner, some significant conclusions have been drawn. The chemical composition suggests that much of the lunar mare (and at least some of the terra) surface material is made up of compounds and minerals that are well-known on earth

(e.g., minerals of the feldspar and pyroxene classes). The composition differs markedly from that of condensed solar material, most meteorites, and terrestrial ultrabasic rocks. The results thus indicate that, for the lunar surface material to have been derived from original solar-system material, that material would have had to undergo large-scale cosmochemical processes that concentrated some elements and removed others before the lunar surface was formed. Presumably it was a process similar to that which produced differentiation of the materials comprising the earth's crust.

The difference established thus far between the terra samples and the mare samples is confined to the lower content of the "iron" group of elements at the terra site. This difference could be significant if it applies generally to the lunar terrae. The "iron" group, at the present stage of data analysis, includes elements which, in general, impart color to rocks. Terrestrial rocks containing larger amounts of these elements are usually darker than rocks having smaller amounts. Thus, the lower content of the "iron" group of elements as found in the *Surveyor VII* samples may be a contributing factor to the brighter appearance of the terrae of the moon (relative to the maria).

Again, if a lower "iron" group content is characteristic of lunar terrae in general, this probably means that the bulk density of the subsurface rocks of the terrae is less than that of comparable material in the maria. In this case, the very gross topographical relationships of the lunar crust would be similar to those of the earth's crust, where, in general, the continental highlands are composed of material less dense than the basaltic ocean bottoms.

References

1. Turkevich, A. L., Franzgrote, E. J., and Patterson, J. H., "Chemical Analysis of the Moon at the Surveyor V Landing Site," *Science*, Vol. 158, pp. 635–637, 1967. Also available as *Surveyor V Mission Report, Part II: Science Results,* Technical Report 32-1246, pp. 119–149. Jet Propulsion Laboratory, Pasadena, Calif., Nov. 1, 1967.

2. Turkevich, A. L., Patterson, J. H., and Franzgrote, E. J., "Chemical Analysis of the Moon at the Surveyor VI Landing Site: Preliminary Results," *Science*, Vol. 160, pp. 1108–1110, 1968. Also available as *Surveyor VI Mission Report. Part II: Science Results,* Technical Report 32-1262, pp. 127–153. Jet Propulsion Laboratory, Pasadena, Calif., Jan. 10, 1968.

3. Franzgrote, E. J., Patterson, J. H., and Turkevich, A. L., "Chemical Analysis of the Moon at the Surveyor VII Landing Site: Preliminary Results," *Surveyor VII Mission Report. Part II: Science Results,* Technical Report 32-1264. Jet Propulsion Laboratory, Pasadena, Calif., Mar. 15, 1968.

III. Future Projects

ADVANCED STUDIES

A. Introduction

The JPL Advanced Studies Office is responsible for the direction, the sponsorship, and, in cooperation with other elements of the Laboratory, the origination of advanced mission and future project studies in applicable areas of interest to the Laboratory. The objective of these studies is to ensure that preliminary technical information and plans for the various potential missions, together with associated information on spacecraft systems, instrumentation systems, launch vehicle systems, resources, and schedules, be available as required. This information can be used primarily for defining specific flight mission programs and as generalized guidance for Laboratory research and advanced development programs.

Each study has been, and will continue to be, documented in a formal final report. This chapter of the SPS, Vol. I, is allocated to provide an abstract or summary of the results of each study, including, where appropriate, reference to the final report for additional details.

B. Long-Range Traverses on the Lunar Surface

1. Introduction

One conclusion of the study of lunar exploration missions reported in SPS 37-49, Vol. I, pp. 65–81, was that long surface traverses would be necessary for sample collection and geological reconnaissance. Therefore, a study was conducted to identify the primary design and operating problems of such missions. Mission criteria were set up in accordance with the stated exploration goals, and a baseline design for a lunar roving vehicle with an earth-based control system was developed. The initial results are presented here.

In studies that are still in progress, efforts are being made to evaluate: (1) the baseline system's performance relative to the stated mission objectives, (2) possible tradeoffs within the baseline concept, (3) the consequences of using a design more or less elaborate than the baseline design, and (4) the areas where the most critical problems in development and operation might be expected to occur.

2. Traverse Mission Criteria

Certain initial assumptions were necessary to derive mission criteria that would be meaningful for a system design:

(1) Local exploration, sample collection, site evaluation, and instrument emplacement by astronauts will be achieved at several widely separated locations in an equatorial zone on the moon's near side. The landing points and approach paths will have few, if any, significant terrain hazards.

(2) Overhead reconnaissance, as begun by the *Ranger* and *Lunar Orbiter* spacecraft, will be extended selectively in area coverage, photometric and dimensional fidelity, spectral and dimensional resolution, and collaboration (e.g., retargeting) during surface missions.

(3) Long traverses will have to be automated because of the high cost and complexity of prolonged manned operations on the lunar surface.

(4) Technical and resource constraints will require that experiments made along the traverse emphasize only the highest-priority scientific goals, and that the early traverses, at least, be entirely within the earth's line-of-sight.

With these assumptions, the stated mission goals led to the conclusion that sample collection (for subsequent return to earth) will be the primary objective of the traverse. Certain *in-situ* measurements will thus be necessary; i.e., it was recognized that the sampling will have to be selective. Other *in-situ* measurements will be considered as desirable secondary objectives. Since one of the major functions of the long traverse will be to seek out and evaluate sites for further investigation, the system will have to have some capability for general reconnaissance.

These objectives result in an instrument complement including the following devices:

(1) Instrumentation for visual observation.

(2) Sample collection, processing, identification, and storage mechanisms.

(3) Chemical or mineral discrimination (primary) and analysis (highly desirable secondary) instruments.

(4) Environmental sensors and systems for precise position determination.

Also, the sensors required for navigation and motion control should be configured to support the exploration mission, and *vice versa*, to the extent practical.

By examining the results of past lunar site surveys, together with studies of the factors expected to limit vehicle mobility on the moon, a nominal net distance of 1500 km was selected. At the expected speed of travel, allowing for limited ground-station availability, lunar night survival, hazard detours, and miscellaneous exploratory activities, this distance will be covered in about 1 yr. This conclusion is predicated on the assumption that long-life and night-survival engineering problems are less complex than the engineering and operational problems associated with travel at more than a walking pace.

3. System Design Considerations

To determine a baseline design, it was decided to investigate the simplest system capable of carrying out the previously described mission. Use was made of data from previous studies of *Surveyor* flight results (Refs. 1–3) and of experience gained in testing *Surveyor* lunar roving vehicles (Fig. 1).

Fig. 1. *Surveyor lunar roving vehicle*

The requirements of the long traverse mission, as defined above, are beyond the performance capacity of the *Surveyor* lunar roving vehicle. The payload weight estimates for larger vehicles (Fig. 2) indicate that vehicles in the 500- to 1000-lb class will be required. Thus, a means for delivering such vehicles to the lunar surface, using existing lunar flight systems, was required.
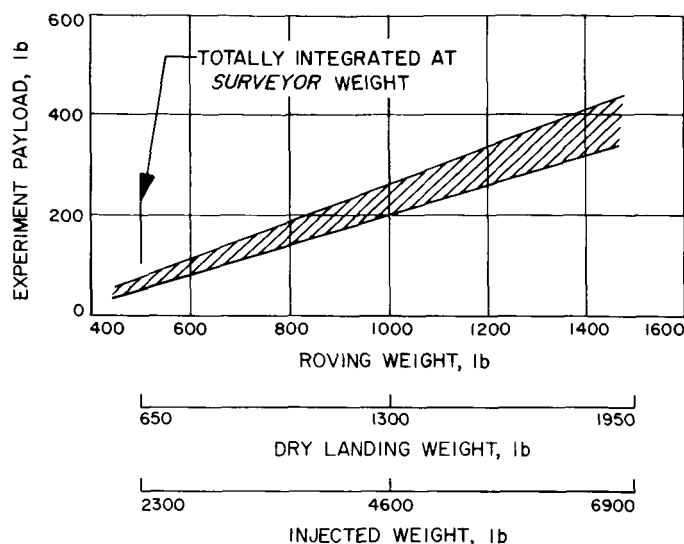

Fig. 2. Experiment payload weight as a function of roving, dry landing, and injected weights

One delivery mode is to carry the roving vehicle as part of the payload of a manned *Apollo* lunar module. Studies of this concept and of the use of the roving vehicle as an astronaut mobility aid were made at the Marshall Space Flight Center and the Manned Spacecraft Center. The results indicate that payload volume and weight constraints of the lunar module may permit carrying a rover of the required size. However, from the standpoint of the traverse mission *per se*, this is a high-cost mode because it involves two *Apollo* lunar flights: one to deliver and launch the rover, and the other to retrieve the collected samples at the end of the traverse.

Another possibility is to increase the size of the *Surveyor* spacecraft/lunar roving vehicle combination (Fig. 3). This would require the use of a new launch vehicle intermediate in size between the *Atlas/Centaur* and the *Saturn V*. This approach is called the "field assistant/science station concept," in which the field assistant is the roving vehicle and the science station is a package of instruments remaining on the landed spacecraft. This design permits both mobile experiments and stationary geophysical measurements during a single
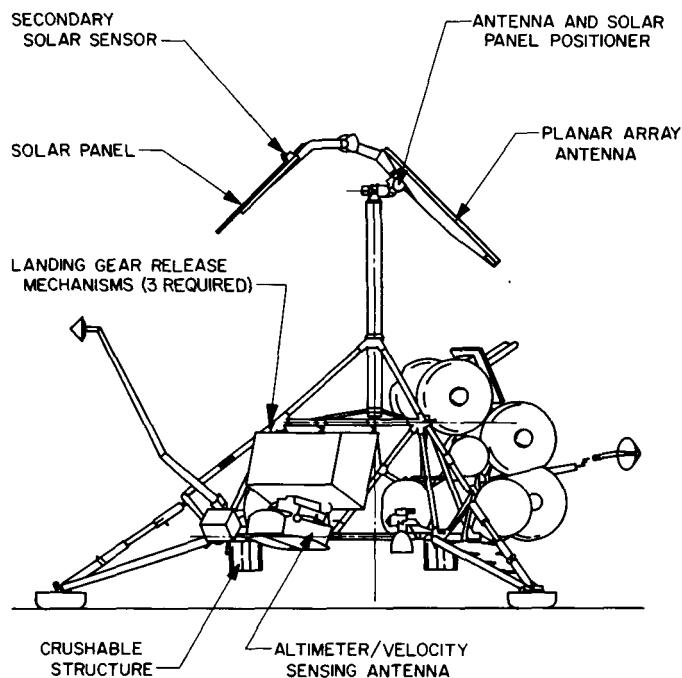

Fig. 3. *Surveyor* lunar roving vehicle installed on spacecraft

mission. However, it requires substantial and costly new developments for the launch vehicle and the delivery spacecraft, as well as for the roving vehicle.

The delivery mode that appears most advantageous, which was thus selected for the baseline design, is one in which the roving vehicle itself constitutes the basic spacecraft structure; it carries not only the subsystems required for the traverse mission, but also those necessary for transit, descent, and landing. Weight and performance calculations show that, by revising the spacecraft structure and exploiting the propulsion and guidance margins found available through experience with the *Surveyor* spacecraft, the present *Atlas/Centaur* and *Surveyor* propulsion systems can deliver to the lunar surface a module with enough weight to provide mobility and an instrument payload of 50 to 100 lb (comparable to that of present *Surveyor* spacecraft). One iteration of the baseline vehicle design, based on a 90-h trajectory, gives the following total weights less payload for the three required configurations:

Configuration	Weight, lb
Flight	2247.15
Descent and landing	2192.72
Travel	447.06

The maximum payload would be 91.01 lb, giving a total separated weight at injection of 2338.16 lb.

A payload of 50 to 100 lb can include not only the mechanisms for the prime sampling function, but also substantial instrumentation for the *in-situ* experiments. However, if no new propulsion system development is assumed, a payload of this magnitude can be achieved only by limiting the weight of other components. Accordingly, investigations were made to determine the minimum acceptable onboard complement of guidance and navigation equipment, to compare types and capacities of the required power subsystems, and to evolve design compromises regarding mobility, hazard sensing, and capabilities of the ground display and command system.

These efforts resulted in the adoption of a baseline navigation concept relying on visual landmark identification as the primary means of locating the vehicle and selecting its course. Assistance would be provided through radio tracking and the angle references obtained by knowledge of the directions to sun and earth with respect to the local vertical. Travel would be in steps, allowing the limited power available to be used mainly for imaging and wide-band communications during stops, and for motive power during movement. Tests are in progress to evaluate the feasibility of this technique in terrain resembling that of the moon.

References

1. *1967 Summer Study of Lunar Science and Exploration, University of California, Santa Cruz, July 31–August 13, 1967*, NASA SP-157. National Aeronautics and Space Administration, Washington.

2. *Lunar Surface Mobility Systems Comparison and Evolution Study (MOBEV), Volume I, Book 1*, Report BSR 1441. Bendix Corp., Ann Arbor, Mich., Oct. 1966.

3. *General Motors Roving Vehicle Motion Control Final Report*, TR 67-60. Work performed under JPL Contract 951829. General Motors Corp., Santa Barbara, Calif., Dec. 1967.

IV. Advanced Planetary Missions Technology
ADVANCED STUDIES

A. Introduction

An Advanced Planetary Missions Technology Program has been established under the cognizance of the JPL Assistant Laboratory Director for Flight Projects. Mission and system studies and scientific and engineering work are being performed to support planning and advance the state-of-the-art applicable to future planetary missions. The current technological activities are reported in this chapter of the SPS, Vol. I.

B. Planetary Vehicle Thermal Insulation System[1]

1. Introduction

Thermal protection systems for interplanetary spacecraft present certain unique design constraints:

(1) Variation in heat load from earth to planetary and interplanetary distances.

(2) Planetary quarantine considerations.

(3) Prolonged exposure to vacuum, ultraviolet, and proton bombardment.

(4) Limitations regarding weight.

---

[1]The work reported herein was performed by General Electric Company under JPL Contract 951537 from October 3, 1966, to April 1, 1968.

In addition, several important factors related to launch vehicle loads must be considered: the effects of shock, vibration and acoustic environments; and the need to vent the insulation system during ascent. Each of the above factors has a direct influence on the type of insulation material and the methods of attachment.

A research and development program was conducted to select, design, fabricate, and test super-insulation systems applicable for use on large planetary vehicles (such as that shown in Fig. 1). The final design was to be, in essence, qualified for interplanetary space vehicles.

2. Study

Candidate insulation materials were evaluated, and a preliminary assessment was made of the vehicle thermal requirements. Tests were performed to determine absorptivity, emissivity, weight loss, and thermal conductivity. Relative to possible sterilization requirements (i.e., planetary quarantine), the materials were exposed to ethylene oxide and dry heat sterilization cycles to evaluate their compatibility with these environments. The effects of high temperatures on insulation, such as might be induced by heat from a rocket motor, were experimentally evaluated, as were the effects of ultraviolet exposure and proton bombardment. On the basis of these tests and evaluations, gold-coated Mylar was selected as the insulation material,
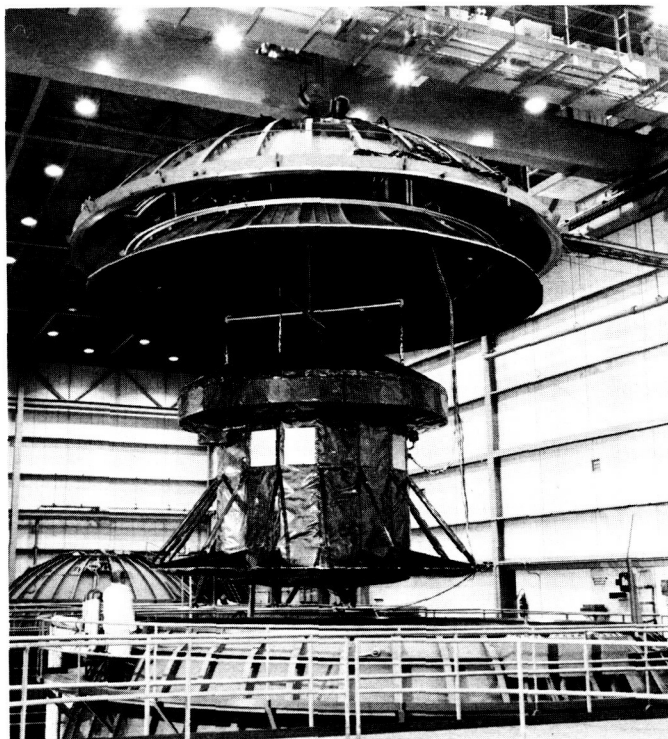
Fig. 1. Planetary vehicle thermal insulation system

because water contained in the ethylene oxide sterilization cycle dissolved the aluminum coating on aluminized Mylar. Heat sterilization of the insulation materials presented no problems.

Tests were also conducted to evaluate the effects of rapid depressurization on insulation blankets of varying sizes. The depressurization pressure–time cycle simulated the conditions expected on a typical ascent trajectory. Thermal analyses evaluated preliminary requirements for thermal insulation of the capsule for seven mission phases and of the spacecraft for five mission phases. It was concluded that 24 layers or less of insulation will provide adequate protection, but that large insulation blankets will require venting.

A study was also performed to assess the advisability of thermal scale modeling of the insulation systems. Such modeling was found to be inadvisable for insulation-system evaluation.

3. Design

A full-scale thermal-vacuum test fixture and the insulation system were designed. Insulation blanket design was based upon the use of vapor-deposited gold on 0.25-mil Mylar and vapor-deposited gold on 0.5-mil Kapton. A detailed thermal analysis of the spacecraft and capsule was performed to aid in the prediction of the thermal-vacuum test results. Steady-state analyses were performed for two external environments: near-earth cruise and Mars orbit. The insulation blanket requirements were generated, and a specification was developed for the procurement of gold on Mylar and Kapton with the required emissivity and adhesion properties. Evaluation tests were also conducted to specify tape materials and adhesives.

Additional depressurization tests were conducted with restraining fasteners and vent holes of several different configurations incorporated into the test blankets. The results of these tests provided guidelines for specifying vent hole and fastening requirements.

Shock, acoustic, and vibration tests were performed on typical test blankets. It was found that both the blankets and fasteners were compatible with the shock, vibration, and acoustic loads. In addition, an insulation blanket was subjected to 60 days of vacuum storage at low temperature, followed by vibration to simulate the start of an orbit insertion motor. Prolonged vacuum storage followed by vibration had no adverse effect on the insulation system, nor was there any measurable change in thermal performance.

4. Fabrication

During fabrication of the full-scale test fixture and the insulation blankets, considerable attention was devoted to techniques for blanket manufacture and attachment to the vehicle that were as efficient and simple as possible. Vent holes were drilled in the insulation materials while still rolled.

A crinkling machine permitted deep crinkling with no removal of the gold coating. As the material was crinkled, it was wrapped upon a large drum; when the proper number of layers was obtained, the material was cut and the blanket was available for sizing. Fixtures were developed which permitted handling of the blankets with relative ease and rapid application to the vehicle. The blankets were held to the skin by means of a fastener that consists of a Velcro hook and pile and a nylon support post. Its holding ability was amply demonstrated during the previous environmental tests. The area and weight of the insulation applied are given in Table 1.

5. Testing

A thermal-vacuum test of the insulated full-scale test fixture was then conducted. Appropriate heater elements

34

Table 1. Area and weight of insulation applied to vehicle

Location	Area, ft²	Weight, lb
Capsule	474	35.3
Spacecraft side and struts	370	25.0
Base (solar array)	65	3.3
Base (around engine)	45	4.7
Spacecraft/capsule separator	119	5.8
Total	1073	74.1

were applied to the vehicle to simulate onboard heat sources. Approximately 180 thermocouples were included to measure temperatures on the vehicle.

Four series of tests were run to evaluate the efficiency of the insulation system. The first three tests were planned to have the capsule and spacecraft portions of the vehicle at or near the same temperatures, namely, 115, 60, and 10°F. The fourth test was structured to provide data for calculating a "capsule off" condition; the planned temperatures were 115°F for the spacecraft and 10°F for the capsule.

The first and second temperature conditions were met. However, in the third test, without any electrical power to the spacecraft bay heaters, the temperature rise was such as to require the spacecraft temperature to be 25°F. For the fourth test it was necessary to adjust the capsule temperature to 25°F instead of 10°F. These changes were necessitated because the actual heat leaks were larger than originally estimated. The gross power (i.e., the electrical power input, adjusted for the heat capacity contribution of the spacecraft or capsule structure) that was required to maintain the test temperatures is shown in Table 2.

Table 2. Gross power required to maintain test temperatures

Temperature, °F		Power, W	
Spacecraft	Capsule	Spacecraft	Capsule
115	115	225	107
60	60	127	66
25	10	−11ᵃ	32
115	25	305	−28ᵃ

ᵃNo electrical power applied.

The capsule is a completely insulated body that has only three concentrated heat leaks or thermal shorts. The major capsule thermal short occurs at the capsule/spacecraft interface. Temperature and power conditions were measured to evaluate heat transfer through these interconnections. The other capsule thermal shorts occur at the four lifting lugs and the capsule/spacecraft electrical harness. These points were instrumented to provide data from which heat leaks could be calculated. The capsule external insulation performance data, as derived from the conditions of the first test, are given below:

Structural temperature change, °F/h	0.156
Structural capacity contribution, W	−11
Electrical power, W	(+) 118
Gross power, W	107
Capsule heat leaks, W External supports (4 W) Wiring harness (1 W) Spacecraft interchange (11 W)	(−) 16
Insulation heat flow (Gross power minus leaks), W	91
Effective emittance at 114°F (average temperature)	0.00352

Figure 2 plots the capsule insulation heat flow as a function of temperature, as derived from the four tests.
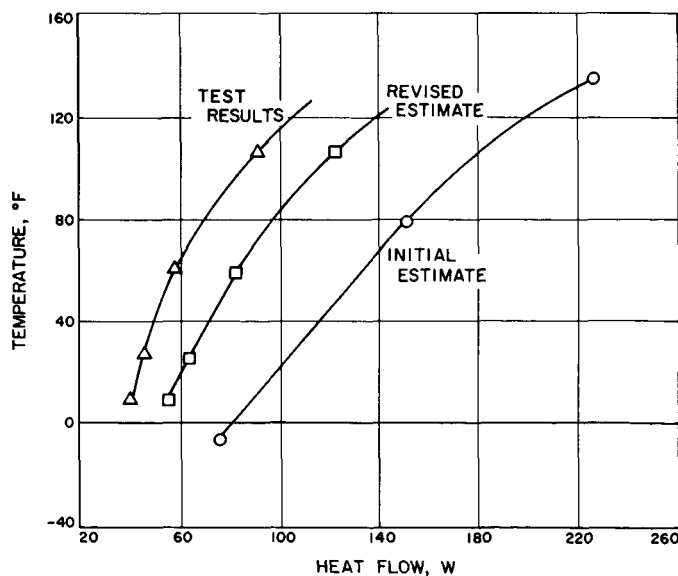

Fig. 2. Capsule insulation heat flow as a function of temperature

In addition, it shows initial predictions based on calorimeter tests of hand-crinkled gold-coated 0.25-mil Mylar and revised predictions based on additional calorimeter tests of more deeply crinkled machine-processed material. Both predicted curves include a 25% degradation factor of the basic calorimeter performance to account for support posts and joints and an additional 50% performance reduction for non-ideal conditions attributable to manufacturing and installation procedures. The actual performance curve shows only about a 39% degradation from calorimeter measurements of the basic unperturbed insulation material.

Capsule insulation effective emittances from the four tests are given below:

Temperature, °F	Effective emittance
114	0.00352
57	0.00331
10	0.00341
25	0.00326

The effective emittances show agreement within a tolerance of ±4% (a high degree of uniformity for a test of this type).

The insulation system performance, as measured by the capsule data, proved to be highly satisfactory. Determination of the capsule insulation performance was relatively simple, but that of the spacecraft performance is considerably more difficult. The external insulation heat flow is small relative to the heat flows from the exposed equipment bay panels, the external solar array support struts and beams, and the base solar array and heater can that simulates solar heating of the base surfaces. There are no calibrated conductances on these heat flow paths, and precise information concerning the heat flow values is not available. Analysis of the data is continuing, but the insulation heat flux determined for the spacecraft will not be as precise as that obtained for the capsule.

However, the overall protection furnished by the spacecraft thermal insulation is excellent. At Mars solar intensity, only a small amount of electrical equipment heat rejection would maintain the spacecraft at a desirable temperature level. It is also evident that the heat rejection range of louvered equipment bay panels would be sufficient to provide satisfactory spacecraft temperatures over the full range of expected spacecraft equipment power. It is thus concluded that the spacecraft would be adequately protected, from a thermal standpoint, for all regimes of the planetary mission. The insulation system is essentially "flight qualified."

## C. Dissociation of Atmospheric Constituents During Planetary Entry

During entry into a planetary atmosphere, the elevated temperatures produced by flow stagnation are sufficient to produce dissociation of atmospheric gases. If an unknown gas mixture having both dissociated and undissociated components is injected into a mass spectrometer on a planetary entry probe, an unambiguous identification of the initial mixture may not be possible due to problems of data interpretation. This is especially true for the detection and identification of trace gases. Thus, the useful operating range of a mass spectrometer system on such a probe may well be limited to those portions of the entry trajectory where the atmospheric constituents will not be appreciably dissociated.

An analysis was performed to identify points along a given trajectory where component dissociation would be appreciable. It was intended to furnish a conservative datum upon which mass spectrometer measurements might be based. The compounds chosen for analysis were those suggested by Wilhite and Hollis (Ref. 1) as possibly being present in a Martian atmosphere. The gases and the reactions considered are given in Table 3, where all

Table 3. Gases and dissociation reactions considered in analysis

Gas	Reaction
Hydrogen	$H_2 \rightleftarrows H + H$
Nitrogen	$N_2 \rightleftarrows N + N$
Oxygen	$O_2 \rightleftarrows O + O$
Carbon monoxide	$CO \rightleftarrows C + O$
Carbon dioxide	$CO_2 \rightleftarrows CO + O$
Methane	$CH_4 \rightleftarrows CH_3 + H$
Water vapor	$H_2O \rightleftarrows OH + H$
Nitric oxide	$NO \rightleftarrows N + O$
Nitrous oxide	$N_2O \rightleftarrows N_2 + O$
Nitrogen dioxide	$NO_2 \rightleftarrows NO + O$
Ammonia	$NH_3 \rightleftarrows NH_2 + H$
Methyl fluoride	$CH_3F \rightleftarrows CH_3 + F$
Methyl chloride	$CH_3Cl \rightleftarrows CH_3 + Cl$
Hydrogen sulfide	$H_2S \rightleftarrows HS + H$
Sulfur dioxide	$SO_2 \rightleftarrows SO + O$

reactions are of the form:

$$A \rightleftarrows B + C$$
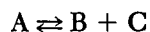
The equilibrium constant for such a reaction, in terms of the partial pressures of the reactants, is given by

$$K_p = \frac{p_B \times p_C}{p_A}$$

In terms of the degree of dissociation α, this becomes

$$K_p = \frac{\alpha^2 P}{1 - \alpha^2}$$

where P is the total pressure of the reactants.

Solving for α gives

$$\alpha = \left(\frac{K_p}{K_p + P} \right)^{1/2}$$

The equilibrium constant K_p is assumed to be independent of pressure, but varying with temperature according to the van't Hoff equation:

$$- \ln K_p = \Delta F^\circ / RT$$

where

ΔF° = the change in free energy that accompanies the reaction

$$= \Sigma (\Delta H + TS)$$

with ΔH representing the heat of formation, T the absolute temperature, and S the entropy of each reactant.

Data from the JPL 1880 trajectory program were used as the starting point in the analysis. These data include the altitude, flight Mach number, ambient density, ambient temperature, and the stagnation point enthalpy along the trajectory. Assuming constant specific heat ratio and specific heat at constant pressure, the total stagnation pressure (calculated from the Rayleigh pitot formula) and the stagnation temperature may be determined along the flight path. Values of ΔH and S are determined from the joint Army–Navy–Air Force (JANAF) thermochemical tables (Ref. 2). For stagnation temperatures greater than 6000°K, the value at 6000°K is used. After the free energy of the reaction is calculated and the equilibrium constant at stagnation temperature and a pressure of 1 atm is determined, the degree of dissocia-

tion at stagnation pressure (or some fraction thereof) may be computed.

The procedure outlined has been applied to the case of a 6.5-ft-diam, 60-deg blunted cone with an 18-in. nose radius entering Mars atmospheres VM-7 and VM-8. The partial pressure of the various constituent gases was varied by factors of ten from 100 to 0.001%, the latter value representing a limiting detection threshold for the mass spectrometer. The results are given in Table 4. The variation with partial pressure of the particular constituent gas of interest is not large. The critical component for each atmosphere is, of course, that gas whose dissociation requires the least energy, i.e., nitrous oxide.

Calculated for the above case, the distribution of the percentage of dissociation for nitrous oxide through the flight trajectory is plotted in Fig. 3. The other gases considered exhibit a similar behavior, with the 0% dissociation points shifted to higher altitudes. It should be
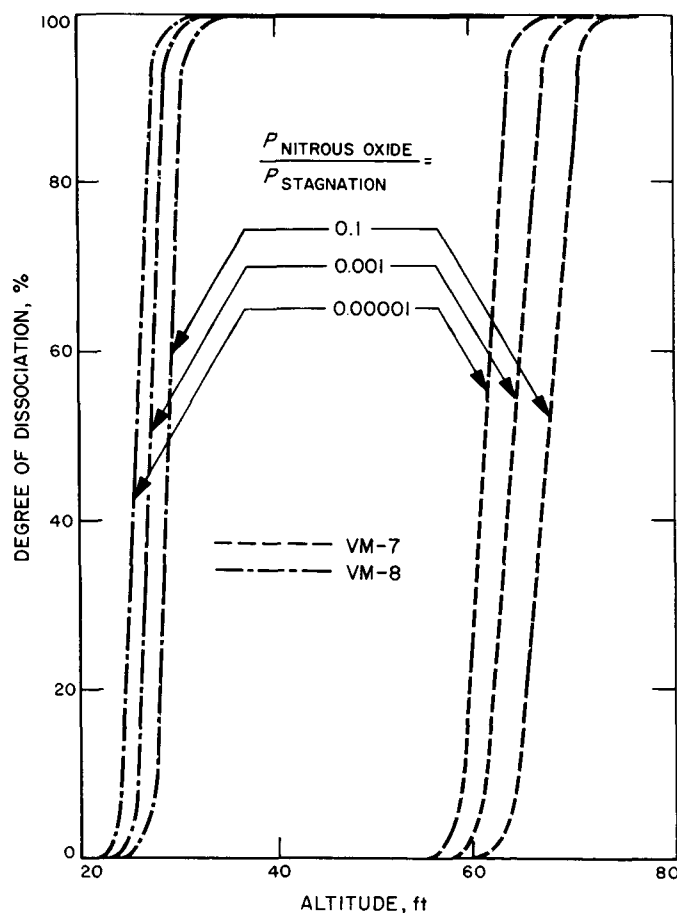

Fig. 3. Dissociation distribution for nitrous oxide in atmospheres VM-7 and VM-8

Table 4. Mach number of constituent gases for atmospheres VM-7 and VM-8, 1 and 10% dissociation

Gas	Mach number for atmosphere VM-7 and indicated variation in partial pressure of constituent gas						Mach number for atmosphere VM-8 and indicated variation in partial pressure of constituent gas					
	100%	10%	1%	0.1%	0.01%	0.001%	100%	10%	1%	0.1%	0.01%	0.001%
	Degree of dissociation = 1%											
Hydrogen	9.99	9.59	9.14	8.76	8.45	8.15	12.47	11.75	11.28	10.64	10.24	9.90
Nitrogen	14.48	13.84	13.26	12.76	12.45	11.92	18.92	18.10	17.11	16.35	15.79	15.04
Oxygen	10.41	9.86	9.46	9.12	8.78	8.46	12.84	12.33	11.58	11.25	10.62	10.25
Carbon monoxide	15.19	14.56	13.97	13.47	13.14	12.61	20.05	19.17	18.24	17.37	16.90	16.04
Carbon dioxide	10.16	9.78	9.33	9.08	8.69	8.44	12.58	12.15	11.44	11.21	10.50	10.22
Methane	9.24	8.96	8.50	8.32	7.87	7.73	11.38	10.89	10.31	10.13	9.41	9.16
Water vapor	10.46	9.94	9.62	9.17	8.94	8.51	13.03	12.40	11.72	11.29	10.80	10.31
Nitric oxide	12.05	11.53	11.12	10.59	10.28	9.84	15.45	14.64	13.80	13.40	12.61	12.32
Nitrous oxide	5.44	5.10	5.00	4.79	4.56	4.39	6.25	6.06	5.72	5.24	5.09	5.04
Nitrogen dioxide	7.75	7.32	7.08	6.84	6.48	6.36	9.25	9.04	8.33	8.11	7.88	7.28
Ammonia	9.55	9.12	8.71	8.43	8.08	7.79	11.71	11.26	10.57	10.21	9.78	9.28
Methyl fluoride	9.39	9.08	8.64	8.41	8.03	7.78	11.54	11.21	10.47	10.19	9.69	9.25
Methyl chloride	8.38	7.88	7.70	7.23	7.06	6.78	10.17	9.46	9.15	8.71	8.24	8.09
Hydrogen sulfide	9.09	8.60	8.37	7.89	7.72	7.30	11.24	10.47	10.16	9.46	9.16	8.92
Sulfur dioxide	10.56	10.12	9.77	9.34	9.09	8.74	13.39	12.54	12.12	11.43	11.22	10.55
	Degree of dissociation = 10%											
Hydrogen	11.19	10.55	10.00	9.60	9.15	8.77	14.16	13.38	12.48	11.76	11.29	10.65
Nitrogen	15.88	15.14	14.48	13.85	13.27	12.77	21.33	20.02	18.93	18.11	17.12	16.36
Oxygen	11.41	10.84	10.41	9.87	9.47	9.13	14.60	13.63	12.85	12.34	11.59	11.41
Carbon monoxide	16.61	15.86	15.19	14.56	13.98	13.47	22.54	21.20	20.06	19.18	18.25	17.38
Carbon dioxide	11.19	10.62	10.17	9.78	9.33	9.22	14.09	13.43	12.60	12.15	11.45	11.27
Methane	10.24	9.76	9.25	8.96	8.51	8.33	12.72	12.11	11.40	10.90	10.33	10.15
Water vapor	11.55	11.00	10.47	9.94	9.62	9.18	14.71	13.75	13.04	12.41	11.73	11.59
Nitric oxide	13.39	12.68	12.05	11.54	11.12	10.59	17.47	16.35	15.45	14.65	13.82	13.48
Nitrous oxide	6.08	5.75	5.44	5.12	5.01	4.79	7.19	6.83	6.26	6.19	5.73	5.26
Nitrogen dioxide	8.52	8.07	7.75	7.33	7.26	6.84	10.39	9.83	9.27	9.05	8.35	8.28
Ammonia	10.55	9.98	9.55	9.13	8.71	8.44	13.37	12.47	11.72	11.49	10.58	10.47
Methyl fluoride	10.43	9.86	9.40	9.09	8.64	8.54	12.97	12.35	11.55	11.28	10.48	10.36
Methyl chloride	9.17	8.68	8.43	7.89	7.73	7.24	11.35	10.59	10.33	9.48	9.36	8.72
Hydrogen sulfide	10.07	9.56	9.10	8.61	8.40	7.90	12.59	11.78	11.25	10.48	10.26	9.48
Sulfur dioxide	11.70	11.13	10.57	10.13	9.78	9.34	14.81	13.92	13.41	12.55	12.12	11.45

noted that the change from 100 to 0% dissociation occurs within an altitude band of 10,000 ft or more. Thus, there appears to be no problem regarding what level of dissociation is acceptable for the initiation of mass spectrometer operation; i.e., the gain in operating time by beginning to sample where a high level of dissociation occurs is negligible.

Also, there is no problem in deciding what effects the concentration of a particular gas might have on the initiation of sampling; again, the altitude band is of the order of 10,000 ft, and the design concentration would have little effect on the initial sample acquisition point. The main concern must be the effect of the overall atmospheric composition. Figure 3 shows the dramatic reduction in altitude of 0% dissociation in going from atmosphere VM-7 to VM-8.

References

1. Wilhite, W. F., and Hollis, O. L., "The Use of Porous Polymer Beads for Analysis of the Martian Atmosphere," *J. Gas Chrom.*, Vol. 6, pp. 84–88, Feb. 1968.

2. *JANAF Thermochemical Data*. Dow Chemical Company, Midland, Mich., 1965.